mutation. Interestingly, the *fad104*-deficient mice died within 1 day of birth. All of the *fad104*-deficient pups at E18.5 were breathing and moving just after caesarean section, suggesting that the disruption of *fad104* caused rapid postnatal death. It is well known that the maintenance of blood glucose levels and the thermoregulation have pivotal roles for survival of newborn pups just after birth [27,28]. However, as shown Fig. 2, *fad104*-deficient neonates did not exhibit the abnormalities about blood glucose level, body temperature, and BAT weight. In our previous reports, *fad104* was found to be highly expressed in white adipose tissue (WAT). On the other hand, *fad104* was also modestly expressed in heart, kidney and lung [12]. Since little WAT is found in newborns, it is possible that the postnatal lethality observed in *fad104*-deficient mice is caused by a functional disorder of *fad104* in organs including the heart, kidney and lung. In order to elucidate the cause of the rapid death after birth of *fad104*-deficient mice, a pathological analysis of these organs is now ongoing.

Kuma et al. indicated that mice deficient for *Atg5*, which is essential for autophagosome formation, die within 1 day at birth, suggesting that autophagic degradation of proteins is important for survival during neonatal starvation [29]. We attempted to examine whether *fad104* is involved in the regulation of autophagic activity. During autophagy, microtubule-associated protein light chain (LC3) is processed from the cytosolic form, LC3-I, to the membrane-bound form, LC3-II. Since the amount of LC3-II correlates with the number of autophagosomes, immnoblotting of endogenous LC3 can be used to measure autophagic activity. Therefore, we performed Western blotting analysis using the cell lysates prepared from wild-type and *fad104*$^{-/-}$ MEFs under nutrition starvation. Commercially available anti-LC3 antibody, which was employed the detection of endogenous LC3 in MEFs was used [30]. However, we could detect neither LC3-I nor LC3-II in the cell lysates prepared from wild-type and *fad104*$^{-/-}$ MEFs, whereas both LC3-I and LC3-II proteins were detected in the cell lysate prepared from HeLa cells under starvation condition as described previously [31]. Although we could not conclude whether *fad104* is related to autophagic activity in this study, it is necessary to elucidate the relationship between *fad104* and autophagic activity by further analyses.

Although it is well known that the proteins containing the fibronectin type III domain localize to the cell surface, the FAD104 localized to the ER, but not the plasma membrane. Therefore, FAD104 may be a novel protein localized to the ER. The proteins found in the ER have an important role of various cellular functions. For example, calreticulin, a Ca^{2+}-binding protein of the ER, influences the cell spread and cell adhesion via the regulation of c-Src activities and vinculin expression [32,33]. Therefore, we next examined whether a novel gene, *fad104*, also is involved in various cellular functions. Analyses of MEFs prepared from *fad104*-deficient mice demonstrated *fad104* to be crucial for cell proliferation, adhesion, spreading and migration.

As shown in Fig. 6, the disruption of *fad104* caused the reduction of the increase of the cell numbers during 6 days after seeding. This result indicates that the proliferation rate of *fad104*$^{-/-}$ MEFs was slightly attenuated than that of wild-type MEFs. *Fad104*-deficient MEFs also exhibited a delay in cell adhesion and cell spreading (Fig. 7). It is necessary to explore the mechanism which *fad104* regulates the cell proliferation.

Cell migration, cell spreading and adhesive properties are regulated by continuous remodeling of the actin cytoskeleton. For example, in cell migration, the actin structures are divided into three steps; the lamelipodial actin network at the leading edge of the cell, filopodial bundles beneath the plasma membrane, and contractile actin stress fibers in the cytoplasm [34]. At the early stage of adipocyte differentiation, the change to the actin organization is very important. Kawaguchi et al. indicated that ADAM12, a disintegrin and metalloprotease, altered the organization of the actin cytoskeleton and extracellular matrix by impairing the function of β1 integrin, and induced differentiation into mature adipocytes [35]. A deficiency of *fad104* dramatically reduces the formation of stress fibers, strongly suggesting that *fad104* also functions as a key regulator of the actin cytoskeleton's organization, and may promote adipogenesis in the early stages of the differentiation process.

Recently, Obholz et al. reported that a fibronectin type III domain containing 3a (FNDC3A) is necessary for adhesion between spermatids and Sertoli cells, and the mutation of *fndc3a* is the cause of male sterility in symplastic spermatids (sys) mice [36]. FNDC3a is closely related to FAD104, since FNDC3a also contains 9 repeats of the fibronectin type III domain and transmembrane domain. It is of interest that FNDC3a is also necessary for mediating adhesion during spermatogenesis. However, FNDC3a does not have a RGD tripeptide sequence in any fibronectin type III domain repeat sequence. In addition, the disruption of FNDC3a does not cause postnatal death. Thus, although FAD104 and FNDC3a are very similar, these two proteins might have distinct and different roles in cellular functions and developmental processes.

In summary, the present study provided some new insights into the functions of a novel gene, *fad104*, namely as essential for the survival of newborns just after birth and as important for cell proliferation, adhesion, spreading and migration. Although further investigation is definitely needed, *fad104* may play an important role in the late stage of embryonic development or neonates after birth via the regulation of cell proliferation, adhesion, spreading and migration. Furthermore, it is possible that *fad104* regulates these cellular functions by altering the actin cytoskeleton's organization. Although we have no information on how *fad104* regulates the survival of neonates or adipocyte differentiation yet, further analyses of *fad104* would help us to understand not only the signaling pathways at the early stage of adipocyte differentiation but also the molecular mechanisms of survival after birth.

Acknowledgments

We thank Dr. Kei Tominaga and Chiharu Kondo for the construction of targeting vectors and screening of positive ES clones. We are grateful to Misaki Fujimura for the construction of fad104 expression plasmid. We also thank Dr. Takashi Ueda for histological analyses. This work was supported in part by grants from the Ministry of Education, Culture, Sports, Science and Technology (MEXT), Japan, Japan Society for the Promotion of Science (JSPS), the grant-in-aid for research in Nagoya City University, and the Takeda Science Foundation.

REFERENCES

[1] P.G. Kopelman, Obesity as a medical problem, Nature 404 (2000) 635–643.
[2] R.P. Brun, J.B. Kim, E. Hu, S. Altiok, B.M. Spiegelman, Adipocyte differentiation: a transcriptional regulatory cascade, Curr. Opin. Cell Biol. 8 (1996) 826–832.

[3] E.D. Rosen, C.J. Walkey, P. Puigserver, B.M. Spiegelman, Transcriptional regulation of adipogenesis, Genes Dev. 14 (2000) 1293–1307.
[4] M. Imagawa, T. Tsuchiya, T. Nishihara, Identification of inducible genes at the early stage of adipocyte differentiation of 3T3-L1 cells, Biochem. Biophys. Res. Commun. 254 (1999) 299–305.
[5] M. Nishizuka, T. Tsuchiya, T. Nishihara, M. Imagawa, Induction of Bach1 and ARA70 gene expression at an early stage of adipocyte differentiation of mouse 3T3-L1 cells, Biochem. J. 361 (2002) 629–633.
[6] M. Nishizuka, K. Honda, T. Tsuchiya, T. Nishihara, M. Imagawa, RGS2 promotes adipocyte differentiation in the presence of ligand for peroxisome proliferator-activated receptor gamma, J. Biol. Chem. 276 (2001) 29625–29627.
[7] M. Nishizuka, E. Arimoto, T. Tsuchiya, T. Nishihara, M. Imagawa, Crucial role of TCL/TC10beta L, a subfamily of Rho GTPase, in adipocyte differentiation, J. Biol. Chem. 278 (2003) 15279–15284.
[8] A. Kitamura, M. Nishizuka, K. Tominaga, T. Tsuchiya, T. Nishihara, M. Imagawa, Expression of p68 RNA helicase is closely related to the early stage of adipocyte differentiation of mouse 3T3-L1 cells, Biochem. Biophys. Res. Commun. 287 (2001) 435–439.
[9] K. Tominaga, Y. Johmura, M. Nishizuka, M. Imagawa, Fad24, a mammalian homolog of Noc3p, is a positive regulator in adipocyte differentiation, J. Cell. Sci. 117 (2004) 6217–6226.
[10] K. Tominaga, T. Kagata, Y. Johmura, T. Hishida, M. Nishizuka, M. Imagawa, SLC39A14, a LZT protein, is induced in adipogenesis and transports zinc, FEBS J. 272 (2005) 1590–1599.
[11] K. Tominaga, C. Kondo, T. Kagata, T. Hishida, M. Nishizuka, M. Imagawa, The novel gene fad158, having a transmembrane domain and leucine-rich repeat, stimulates adipocyte differentiation, J. Biol. Chem. 279 (2004) 34840–34848.
[12] K. Tominaga, C. Kondo, Y. Johmura, M. Nishizuka, M. Imagawa, The novel gene fad104, containing a fibronectin type III domain, has a significant role in adipogenesis, FEBS Lett. 577 (2004) 49–54.
[13] Y. Johmura, S. Osada, M. Nishizuka, M. Imagawa, FAD24 acts in concert with histone acetyltransferase HBO1 to promote adipogenesis by controlling DNA replication, J. Biol. Chem. 283 (2008) 2265–2274.
[14] D. Craig, M. Gao, K. Schulten, V. Vogel, Structural insights into how the MIDAS ion stabilizes integrin binding to an RGD peptide under force, Structure 12 (2004) 21–30.
[15] R. Pankov, K.M. Yamada, Fibronectin at a glance, J. Cell. Sci. 115 (2002) 3861–3863.
[16] S.K. Sastry, K. Burridge, Focal adhesions: a nexus for intracellular signaling and cytoskeletal dynamics, Exp. Cell Res. 262 (2000) 25–36.
[17] B.H. Geiger, A. Bershadsky, R. Pankov, K.M. Yamada, Transmembrane crosstalk between the extracellular matrix–cytoskeleton crosstalk, Nat. Rev. Mol. Cell Biol. 2 (2002) 793–805.
[18] R.D. Bowditch, M. Hariharan, E.F. Tominna, J.W. Smith, K.M. Yamada, E.D. Getzoff, M.H. Ginsberg, Identification of a novel integrin binding site in fibronectin. Differential utilization by beta 3 integrins, J. Biol. Chem. 269 (1994) 10856–10863.
[19] T. Nagai, N. Yamakawa, S. Aota, S.S. Yamada, S.K. Akiyama, K. Olden, K.M. Yamada, Monoclonal antibody characterization of two distant sites required for function of the central cell-binding domain of fibronectin in cell adhesion, cell migration, and matrix assembly, J. Cell Biol. 114 (1991) 1295–1305.
[20] B.M. Spiegelman, S.D. Farmer, Decreases in tubulin and actin gene expression prior to morphological differentiation of 3T3 adipocytes, Cell 29 (1982) 53–60.
[21] B.M. Spiegelman, C.A. Ginty, Fibronectin modulation of cell shape and lipogenic gene expression in 3T3-adipocytes, Cell 35 (1983) 657–666.
[22] L. Yang, L. Wang, Y. Zheng, Gene targeting of Cdc42 and Cdc42GAP affirms the critical involvement of Cdc42 in filopodia induction, directed migration, and proliferation in primary mouse embryonic fibroblasts, Mol. Biol. Cell 17 (2006) 4675–4685.
[23] F. Chen, Y. Lu, V. Castranova, Z. Li, M. Karin, Loss of IKKβ promotes migration and proliferation of mouse embryo fibroblast cells, J. Biol. Chem. 281 (2006) 37142–37149.
[24] T. Tanaka, N. Yoshida, T. Kishimoto, S. Akira, Defective adipocyte differentiation in mice lacking the C/EBPbeta and/or C/EBPdelta gene, EMBO J. 16 (1997) 7432–7443.
[25] N. Kubota, Y. Terauchi, H. Miki, H. Tamemoto, T. Yamauchi, K. Komeda, S. Satoh, R. Nakano, C. Ishii, T. Sugiyama, K. Eto, Y. Tsubamoto, A. Okuno, K. Murakami, H. Sekihara, G. Hasegawa, M. Naito, Y. Toyoshima, S. Tanaka, K. Shiota, T. Kitamura, T. Fujita, O. Ezaki, S. Aizawa, R. Nagai, K. Tobe, S. Kimura, T. Kadowaki, PPAR gamma mediates high-fat diet-induced adipocyte hypertrophy and insulin resistance, Mol. Cell 4 (1999) 597–609.
[26] J.B. Kim, B.M. Spiegelman, ADD1/SREBP1 promotes adipocyte differentiation and gene expression linked to fatty acid metabolism, Genes Dev. 10 (1996) 1096–1107.
[27] B. Cannon, J. Nedergaard, Brown adipose tissue: function and physiological significance, Physiol. Rev. 84 (2004) 277–359.
[28] M.E. Symonds, M.A. Lomax, Material and environmental influences on thermoregulation in the neonate, Proc. Nutr. Soc. 51 (1992) 165–172.
[29] A. Kuma, M. Hatano, M. Matsui, A. Yamamoto, H. Nakaya, T. Yoshimori, Y. Ohsumi, T. Tokuhisa, N. Mizushima, The role of autophagy during the early neonatal starvation period, Nature 432 (2004) 1032–1035.
[30] C.P. Cheng, M.C. Yang, H.S. Liu, Y.S. Lin, H.Y. Lei, Concanavalin A induces autophagy in hepatoma cells and has a therapeutic effect in a murine in situ hepatoma model, Hepatology 45 (2007) 286–296.
[31] Y. Kabeya, N. Mizushima, T. Ueno, A. Yamamoto, T. Kirisako, T. Noda, E. Kominami, Y. Ohsumi, T. Yoshimori, LC3, a mammalian homologue of yeast Apg8p, is localized in autophagosome membranes after processing, EMBO J. 19 (2000) 5720–5728.
[32] S. Papp, M.P. Fadel, H. Kim, C.A. McCulloch, M. Opas, Calreticulin affects fibronectin-based cell-substratum adhesion via the regulation of c-Src activity, J. Biol. Chem. 282 (2007) 16585–16598.
[33] M. Opas, M.S. Pawlikowski, G.K. Jass, N. Mesaeli, M. Michalak, Calreticulin modulates cell adhesiveness via regulation of vinculin expression, J. Cell Biol. 135 (1996) 1913–1923.
[34] P. Hatulainen, P. Lappalainen, Stress fibers are generated by two distinct actin assembly mechanisms in motile cells, J. Cell Biol. 173 (2006) 383–394.
[35] N. Kawaguchi, C. Sundberg, M. Kveiborg, B. Moghadaszadeh, M. Asmar, N. Dietrich, C.K. Thodeti, F.C. Nielson, P. Moller, A.M. Mercurio, R. Albrechtsen, U.M. Wewer, ADAM12 induces actin cytoskeleton and extracellular matrix reorganization during early adipocyte differentiation by regulating beta1 integrin function, J. Cell. Sci. 116 (2003) 3893–3904.
[36] K.L. Obholz, A. Akopyan, K.G. Waymire, G.R. MacGregor, FNDC3A is required for adhesion between spermatids and Sertoli cells, Dev. Biol. 298 (2006) 498–513.

Cyclin A–Cdk1 regulates the origin firing program in mammalian cells

Yuko Katsuno[a], Ayumi Suzuki[a], Kazuto Sugimura[b], Katsuzumi Okumura[b], Doaa H. Zineldeen[a], Midori Shimada[a], Hiroyuki Niida[a], Takeshi Mizuno[c], Fumio Hanaoka[c,d], and Makoto Nakanishi[a,1]

[a]Department of Cell Biology, Graduate School of Medical Sciences, Nagoya City University, 1 Kawasumi, Mizuho-cho, Mizuho-ku, Nagoya 467-8601, Japan; [b]Laboratory of Molecular and Cellular Biology, Graduate School of Bioresources, Mie University, 1577 Kurimamachiya-cho, Tsu, Mie 514-8507, Japan; [c]Cellular Physiology Laboratory, RIKEN Discovery Research Institute, and Solution Oriented Research for Science and Technology, Science and Technology Corporation, Wako, Saitama 351-0198, Japan; and [d]Faculty of Science, Gakushuin University, Toshima, Tokyo 171-8588, Japan

Edited by Tak Wah Mak, University of Toronto, Toronto, Canada, and approved January 12, 2009 (received for review September 18, 2008)

Somatic mammalian cells possess well-established S-phase programs with specific regions of the genome replicated at precise times. The ATR–Chk1 pathway plays a central role in these programs, but the mechanism for how Chk1 regulates origin firing remains unknown. We demonstrate here the essential role of cyclin A2–Cdk1 in the regulation of late origin firing. Activity of cyclin A2–Cdk1 was hardly detected at the onset of S phase, but it was obvious at middle to late S phase under unperturbed condition. Chk1 depletion resulted in increased expression of Cdc25A, subsequent hyperactivation of cyclin A2–Cdk1, and abnormal replication at early S phase. Hence, the ectopic expression of cyclin A2–Cdk1AF (constitutively active mutant) fusion constructs resulted in abnormal origin firing, causing the premature appearance of DNA replication at late origins at early S phase. Intriguingly, inactivation of Cdk1 in temperature-sensitive Cdk1 mutant cell lines (FT210) resulted in a prolonged S phase and inefficient activation of late origin firing even at late S phase. Our results thus suggest that cyclin A2–Cdk1 is a key regulator of S-phase programs.

Chk1 | DNA replication | molecular combing | ATR protein | checkpoint

Duplication of the eukaryotic genome is regulated by multiple elements including initiation of DNA replication, rate of fork progression, stability of replication forks, and the origin firing program (1). Replication origins are fired in small groups that are activated together within individual replication factories and thus can be visualized as foci (2). Replication origins in a single replication factory are actually comprised of several candidate origins, most of which are not normally used through the mechanism by which firing of 1 origin inhibits activation of any other Mcm2–7 complexes within that factory (3). Thus, S-phase programs appear to be regulated by 2 distinct levels of origin firing; one is the sequential activation of replicon clusters characterized as visible replication foci, and the other is the selection of 1 Mcm2–7 complex around the ORC within a single replication factory.

The DNA replication checkpoint system was reported to be involved in the origin firing program in vertebrate cells (4). In analysis using *Xenopus* egg extract, ATR/Chk1 was shown to regulate the sequential activation of early and late replication origins (5). Chk1 also regulates the density of active replication origins during S phase of avian cells (6). Therefore, ATR/Chk1 may be involved in the regulation of sequential activation of replicon clusters and selection of origins within a single replication factory. Chk1 has been shown to regulate the physiological turnover of Cdc25A and its phosphatase activity, which in turn regulates several cyclin–Cdk activities (7) that are prerequisite for origin firing throughout S phase.

In budding yeast, Clb5-dependent Cdk activity is indispensable for activation of late replication origins (8), suggesting the existence of a specific transfactors for late origin activation in other eukaryotes. In fission yeast, however, clear late origins have not been characterized (9) and replication origins fire stochastically (10, 11). As for mammals, although almost half of origins are activated equally throughout S-phase progression (12), stable subunits of chromosomes equivalent to replication foci maintain their replication timing from S phase to S phase (13).

In this article, we demonstrate that Chk1 depletion resulted in an aberrant origin firing and a hyperactivation of cyclin A2–Cdk1 at early S phase. Ectopic expression of cyclin A2–Cdk1AF induced late origin firing at early S phase, and a loss of Cdk1 activity compromised activation of late origins at late S phase. Our results thus suggested that cyclin A2–Cdk1 might function as a transregulator of late origin firing in mammals.

Results

Chk1 Depletion Results in an Aberrant Origin Firing and a Hyperactivation of Cyclin A2–Cdk1 at Early S Phase. $Chk1^{lox/-}$ mouse embryonic fibroblasts (MEFs) were infected with adenoviruses expressing either LacZ or Cre and synchronized into G_0 phase by serum starvation (14). $Chk1^{lox/-}$ and $Chk1^{del/-}$ MEFs were then stimulated by 15% serum and double-labeled with iododeoxyuridine (IdU) and chlorodeoxyuridine (CIdU) at the indicated times, and their spatiotemporal patterns of replication sites were examined. The mammalian S phase is structured so that the sequential activation of replicon clusters occurs at spatially adjacent sites (15). This spatial relationship is maintained in $Chk1^{lox/-}$ MEFs (Fig. 1*A*), where 86.6 ± 4.4 of foci showed colocalization visualized as yellow color. In contrast, colocalization was detected only at 53.9 ± 4.8 of foci in $Chk1^{del/-}$ MEFs (Fig. 1*B*), indicating that Chk1 depletion in mammals resulted in the aberrant origin firing as observed in avian cells (6). Molecular combing of single DNA molecules was performed to visualize individual origin activation, measure the fork elongation, and define replication structures (Fig. 1*C* and Fig. S1). In asynchronized $Chk1^{lox/-}$ MEFs infected with control LacZ adenoviruses interorigin spacing (90.4 kb on average) was similar to that in mock-infected cells. Chk1 depletion resulted in a clear reduction in origin spacing (34.8 kb on average)(Fig. 1*C Top*). Spatiotemporal pattern of replication sites could also be affected by fork elongation. Chk1 depletion reduced the rate of fork elongation throughout the labeling period (Fig. 1*C Middle*).

Double-labeling protocol also defines 5 classes of replication structure as described (6). Chk1 depletion resulted in a significant reduction in a proportion of consecutively elongating forks (class 1) and an increase in number of new firing initiation during the first (class 2) and second (class 4) labeling period (Fig. 1*C Bottom*). A dramatic increase in the frequency of closely-spaced active origins

Author contributions: M.N. designed research; Y.K., A.S., K.S., K.O., D.H.Z., M.S., and H.N. performed research; T.M. and F.H. contributed new reagents/analytic tools; Y.K., K.S., and M.N. analyzed data; and Y.K. and M.N. wrote the paper.

The authors declare no conflict of interest.

This article is a PNAS Direct Submission.

[1]To whom correspondence should be addressed. E-mail: mkt-naka@med.nagoya-cu.ac.jp.

This article contains supporting information online at www.pnas.org/cgi/content/full/0809350106/DCSupplemental.

www.pnas.org/cgi/doi/10.1073/pnas.0809350106

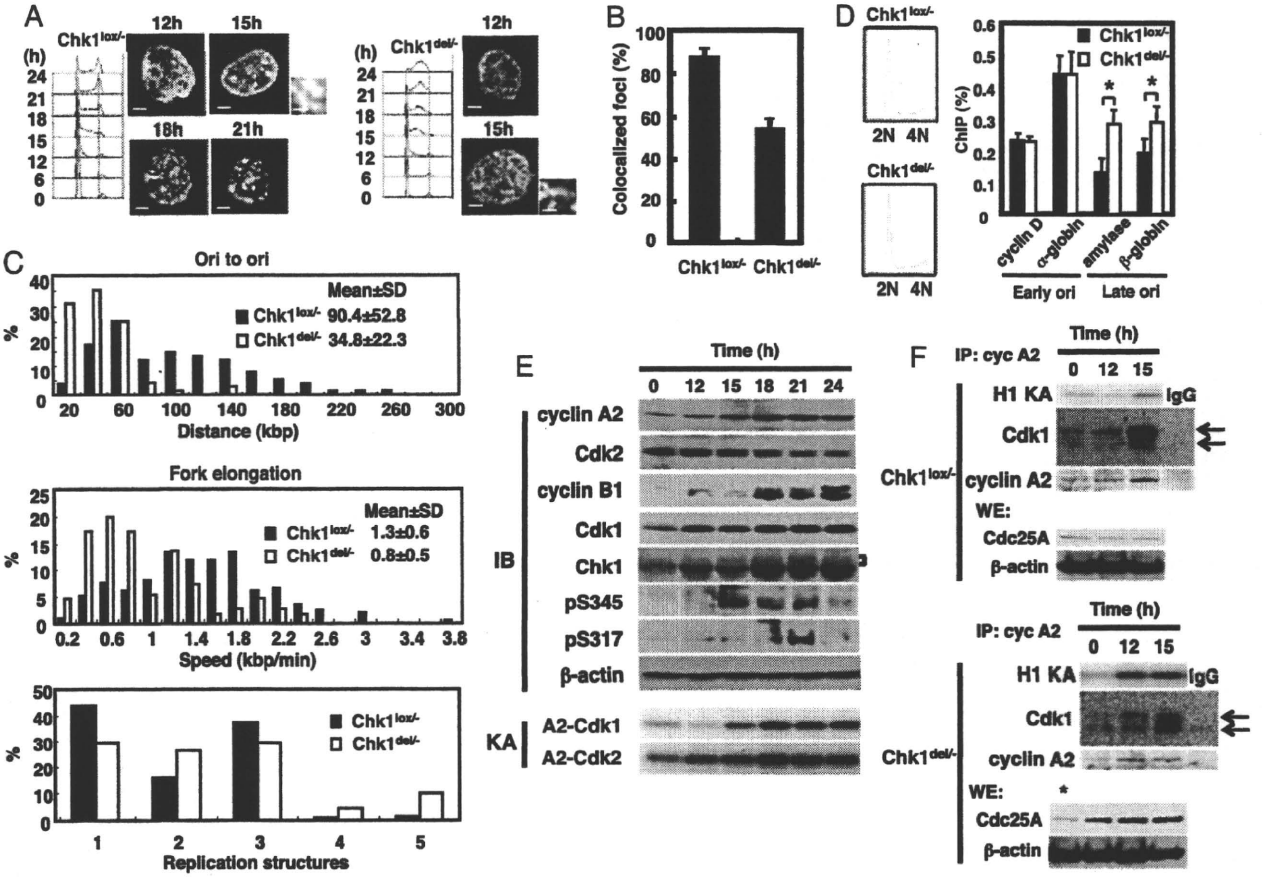

Fig. 1. Chk1 depletion results in an aberrant S-phase program and an activation of cyclin A2–Cdk1 at early S phase. (*A*) Chk1$^{lox/-}$ and Chk1$^{del/-}$ MEFs were synchronized at quiescence by serum starvation and then released by the addition of 15% serum. Cells were harvested at the indicated times, and their cell cycle distributions were analyzed by FACS. Replication sites were pulse-labeled for 15 min with 100 μM IdU and then for 15 min with 100 μM CldU, and analyzed with a Zeiss LSM5 confocal fluorescence microscope. Typical patterns of replication sites at the indicated times are presented. High-power details are from the boxed areas shown. (Scale bars: 5 and 0.5 μm in detail.) (*B*) Colocalization of IdU and CldU foci in Chk1$^{lox/-}$ and Chk1$^{del/-}$ MEFs. Relative colocalization of IdU and CldU foci was determined as a percentage of total foci in both cells ($n > 30$). Data are means ± SD of at least 3 independent experiments. (*C*) Asynchronized Chk1$^{lox/-}$ MEFs were infected with the indicated adenoviruses and double-labeled with IdU and CldU before harvesting at 28 h after infection. Replication structures were visualized by means of dynamic molecular combing. Adjacent origins in replicon clusters (Ori to ori), fork elongation, and replication structure defined by ref. 6 were determined ($n > 100$). Frequency histograms show the distribution of separation in distance (kbp), speed (kbp/min), and replication structure (1, elongating fork; 2, fork growing from 1 ori; 3, terminal fusions; 4, isolated; 5, interspersed). (*D*) Asynchronized Chk1$^{lox/-}$ MEFs were infected with adenoviruses expressing either LacZ or Cre. Cells were labeled with BrdU for 1 h before harvesting at 28 h after infection, and the cell cycle profiles were then analyzed by FACS. Early S-phase fraction indicated by bars was sorted, and nascent DNA was enriched by immunoprecipitation using α-BrdU. The indicated genes were amplified by quantitative PCR, and the results are presented as a percentage of mtDNA. Data are means ± SD of at least 3 independent experiments. Statistical significance was assessed by Student's *t* test (*, $P < 0.01$). (*E*) Synchronized Chk1$^{lox/-}$ MEFs as in *A* were harvested at the indicated times, and the lysates were subjected to immunoblotting by using the indicated antibodies or to an in vitro kinase assay (KA) for cyclin A2–Cdk1 and cyclin A2–Cdk2 with HH1 (2 μg) as a substrate. (*F*) Synchronized Chk1$^{lox/-}$ and Chk1$^{del/-}$ MEFs as in *A* were harvested at the indicated times, and the lysates were immunoprecipitated by using α-cyclin A2 antibodies after 3 times preabsorbance with α-Cdk2. The resultant immunoprecipitates (IP: cyclin A2) or whole-cell extracts (WE) were subjected to immunoblotting or in vitro kinase assay as in *E*. Arrows indicate the fast (active) or slow (inactive) migrated bands of Cdk1. An asterisk represents cell lysates from Chk1$^{lox/-}$ MEFs at 15 h.

(class 5) was observed. These observations suggest that loss of Chk1 frequently stalls and collapses active forks.

We next examined whether Chk1 regulates global sites of DNA synthesis by quantitative ChIP using FACS-based cell sorting (16). To avoid unexpected effects from gross changes in cell cycle profile on this analysis, we analyzed Chk1$^{del/-}$ MEFs 28 h after adenoviral infection, the time at which Chk1 was completely depleted, but the cell cycle profile was almost the same as that of Chk1$^{lox/-}$ cells (Fig. 1*D*). Cells from the first third of S phase were collected (Fig. 1*D Left*). Nascent (BrdU-containing) DNA was enriched by immunoprecipitation using α-BrdU antibodies and amplified by quantitative PCR with specific primers for cyclin D and α-globin for early-replicating DNA and primers for amylase and β-globin for late-replicating DNA. We also monitored amplification of mtDNA as a control, which replicates throughout the cell cycle and is equally represented in nascent DNA preparations (16, 17). The relative amounts of early replication (cyclin D and α-globin) in Chk1$^{del/-}$ MEFs were almost the same as those in Chk1$^{lox/-}$ cells, whereas those of late replication (amylase and β-globin) in Chk1$^{del/-}$ MEFs were significantly higher than those in Chk1$^{lox/-}$ cells (Fig. 1*D Right*). Given that 1 cell possesses ≈1,000 copies of mitochondrial genome, but they replicate throughout the cell cycle, relative amplification of nascent DNA (≈0.3) for early and late origins appeared consistent.

Chk1 is phosphorylated during unperturbed S phase (18, 19), which regulates the activity and stability of Cdc25 phosphatases, leading to the inactivation of Cdks through increased phosphorylation of their Y15 residues (20). Thus, we speculated that Chk1

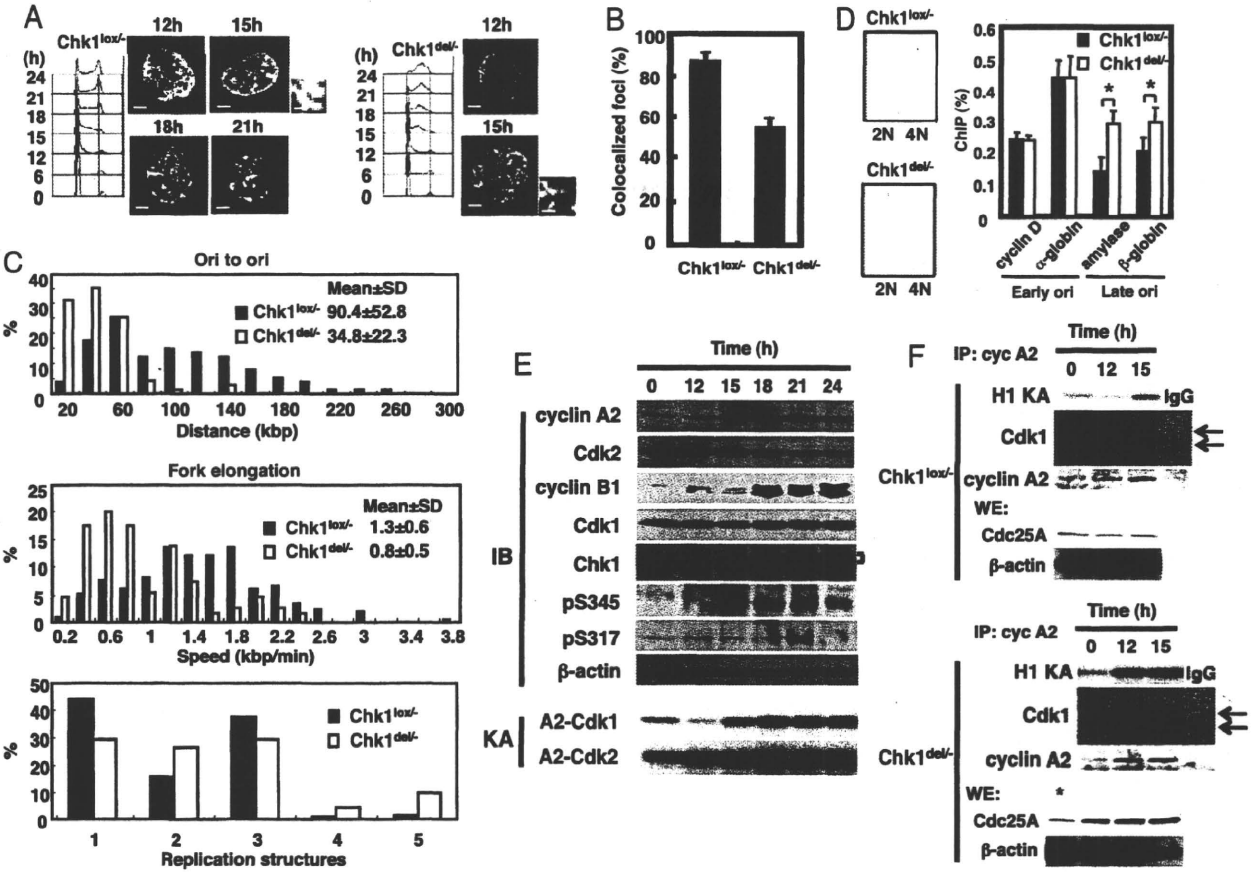

Fig. 1. Chk1 depletion results in an aberrant S-phase program and an activation of cyclin A2–Cdk1 at early S phase. (*A*) Chk1$^{lox/-}$ and Chk1$^{del/-}$ MEFs were synchronized at quiescence by serum starvation and then released by the addition of 15% serum. Cells were harvested at the indicated times, and their cell cycle distributions were analyzed by FACS. Replication sites were pulse-labeled for 15 min with 100 μM IdU and then for 15 min with 100 μM CldU, and analyzed with a Zeiss LSM5 confocal fluorescence microscope. Typical patterns of replication sites at the indicated times are presented. High-power details are from the boxed areas shown. (Scale bars: 5 and 0.5 μm in detail.) (*B*) Colocalization of IdU and CldU foci in Chk1$^{lox/-}$ and Chk1$^{del/-}$ MEFs. Relative colocalization of IdU and CldU foci was determined as a percentage of total foci in both cells ($n > 30$). Data are means ± SD of at least 3 independent experiments. (*C*) Asynchronized Chk1$^{lox/-}$ MEFs were infected with the indicated adenoviruses and double-labeled with IdU and CldU before harvesting at 28 h after infection. Replication structures were visualized by means of dynamic molecular combing. Adjacent origins in replicon clusters (Ori to ori), fork elongation, and replication structure defined by ref. 6 were determined ($n > 100$). Frequency histograms show the distribution of separation in distance (kbp), speed (kbp/min), and replication structure (1, elongating fork; 2, fork growing from 1 ori; 3, terminal fusions; 4, isolated; 5, interspersed). (*D*) Asynchronized Chk1$^{lox/-}$ MEFs were infected with adenoviruses expressing either LacZ or Cre. Cells were labeled with BrdU for 1 h before harvesting at 28 h after infection, and the cell cycle profiles were then analyzed by FACS. Early S-phase fraction indicated by bars was sorted, and nascent DNA was enriched by immunoprecipitation using α-BrdU. The indicated genes were amplified by quantitative PCR, and the results are presented as a percentage of mtDNA. Data are means ± SD of at least 3 independent experiments. Statistical significance was assessed by Student's *t* test (*, $P < 0.01$). (*E*) Synchronized Chk1$^{lox/-}$ MEFs as in *A* were harvested at the indicated times, and the lysates were subjected to immunoblotting by using the indicated antibodies or to an in vitro kinase assay (KA) for cyclin A2–Cdk1 and cyclin A2–Cdk2 with HH1 (2 μg) as a substrate. (*F*) Synchronized Chk1$^{lox/-}$ and Chk1$^{del/-}$ MEFs as in *A* were harvested at the indicated times, and the lysates were immunoprecipitated by using α-cyclin A2 antibodies after 3 times preabsorbance with α-Cdk2. The resultant immunoprecipitates (IP: cyclin A2) or whole-cell extracts (WE) were subjected to immunoblotting or in vitro kinase assay as in *E*. Arrows indicate the fast (active) or slow (inactive) migrated bands of Cdk1. An asterisk represents cell lysates from Chk1$^{lox/-}$ MEFs at 15 h.

(class 5) was observed. These observations suggest that loss of Chk1 frequently stalls and collapses active forks.

We next examined whether Chk1 regulates global sites of DNA synthesis by quantitative ChIP using FACS-based cell sorting (16). To avoid unexpected effects from gross changes in cell cycle profile on this analysis, we analyzed Chk1$^{del/-}$ MEFs 28 h after adenoviral infection, the time at which Chk1 was completely depleted, but the cell cycle profile was almost the same as that of Chk1$^{lox/-}$ cells (Fig. 1*D*). Cells from the first third of S phase were collected (Fig. 1*D Left*). Nascent (BrdU-containing) DNA was enriched by immunoprecipitation using α-BrdU antibodies and amplified by quantitative PCR with specific primers for cyclin D and α-globin for early-replicating DNA and primers for amylase and β-globin for late-replicating DNA. We also monitored amplification of mtDNA as a control, which replicates throughout the cell cycle and is equally represented in nascent DNA preparations (16, 17). The relative amounts of early replication (cyclin D and α-globin) in Chk1$^{del/-}$ MEFs were almost the same as those in Chk1$^{lox/-}$ cells, whereas those of late replication (amylase and β-globin) in Chk1$^{del/-}$ MEFs were significantly higher than those in Chk1$^{lox/-}$ cells (Fig. 1*D Right*). Given that 1 cell possesses ≈1,000 copies of mitochondrial genome, but they replicate throughout the cell cycle, relative amplification of nascent DNA (≈0.3) for early and late origins appeared consistent.

Chk1 is phosphorylated during unperturbed S phase (18, 19), which regulates the activity and stability of Cdc25 phosphatases, leading to the inactivation of Cdks through increased phosphorylation of their Y15 residues (20). Thus, we speculated that Chk1

regulates origin firing program through affecting certain cyclin–Cdks activities. The band corresponding to Chk1 was shifted upward at 15 h and thereafter. This band shift was reversed by phosphatase treatment, indicating that the modification was caused by phosphorylation. Chk1 phosphorylation was also confirmed by using phospho-specific antibodies to Chk1 at Ser-317 and Ser-345 (Fig. 1*E*).

Cyclin A2–Cdk1 activity was first detected at 15 h (middle S phase) and increases thereafter. Cyclin A2–Cdk2 was detected at 6 h (early S phase) and reached maximum at 18 h (Fig. 1*E* and Fig. S2*A*). These results are consistent with the recent report that cyclin A2 starts to form a complex with Cdk1 at mid-S phase (21). Cyclin A2–Cdk1 activity was detected earlier and enhanced in $Chk1^{del/-}$ MEFs when compared with $Chk1^{lox/-}$ MEFs (Fig. 1*F*), where immunodepletion of Cdk2 was equally achieved in both cyclin A2 immunoprecipitates (Fig. S2*B*). Cyclin A2–Cdk2 activity was not apparently affected by Chk1 depletion (Fig. S2*A*). Intriguingly, the amount of Cdc25A was highly elevated in $Chk1^{del/-}$ MEFs. Consistent with this increase in amount of Cdc25A, fast mobility band (active; Y15 dephosphorylation) and slow band (inactive; Y15 phosphorylation) of Cdk1 protein were dominant in those from $Chk1^{del/-}$ MEFs and $Chk1^{lox/-}$ MEFs, respectively (Fig. 1*F*). Specificity of cyclin A2–Cdk1 activity was confirmed by Cdk1 knockdown experiment, where cyclin A2–Cdk1 activities in both MEFs were significantly reduced after Cdk1 depletion (Fig. S3). To further confirm the functional interaction between Chk1 and cyclin A2–Cdk1, $Chk1^{lox/-}$ MEFs were treated with UV light, which phosphorylated Chk1 in an ATR-dependent manner. Chk1 phosphorylation was correlated with the reduction of Cdc25A, the appearance of slow mobility band of Cdk1 protein, and inhibition of cyclin A2–Cdk1 activity (Fig. S4). Taken together, cyclin A2–Cdk1 is likely to be a target of Chk1 through regulation of Cdc25A.

Aberrant Origin Firing in Cells Expressing Cyclin A2–Cdk1AF Fusion Protein. To examine the role of each cyclin–Cdk complex in the origin firing program, we generated a cyclin A2–Cdk1 fusion construct. Because cyclin–Cdk activities are regulated mainly by the phosphorylation of Y15, we generated a constitutively active mutant (CdkAF) in which residues at inhibitory phosphorylation sites were replaced with alanine and phenylalanine and therefore the mutant was not affected by the Chk1–Cdc25 pathway. Recombinant cyclin A2–Cdk2AF, cyclin A2–Cdk1AF, and cyclin B1–Cdk1AF complexes and the fusion proteins were examined for their enzymatic kinetics by using histone H1 (HH1) and lamin B as substrates. Dose-dependent increases in activities of both cyclin–Cdks complex and their fusion proteins were observed (Fig. 2*A*). The kinetic values of these complexes were the same as those of the fusion proteins (Table S1).

Expression of cyclin B1–Cdk1AF, but not cyclin A2–Cdk2AF or cyclin A2–Cdk1AF, induced γH2AX foci in HeLa cells (Fig. 2*B*). Amounts of cyclin B1–Cdk1AF, cyclin A2–Cdk1, and cyclin A2–Cdk2 fusion proteins expressed at 24 h after infection were almost equal to endogenous Cdk1 and Cdk2 proteins, respectively (Fig. 2*C* and Fig. S5). Again, γH2AX was not detected by immunoblotting in cells expressing cyclin A2–Cdk1 or cyclin A2–Cdk2 fusion protein.

Expression of cyclin A2–Cdk1AF and cyclin A2–Cdk2AF fusion protein at the endogenous level did not appear to affect the gross progression of S phase (Fig. 3*A*) although they arrested the cell cycle at M phase because of their inability to be degraded by APC-C at mitosis and thus mitotic exit was inhibited. The expression of cyclin A2–Cdk1AF fusion protein caused the appearance of late replication sites during early S phase when cells were double-labeled with IdU and CIdU (Fig. 3*B*). Dynamic molecular combing revealed that expression of cyclin A2–Cdk1AF fusion protein reduced origin spacing (75.0 kb on average), whereas that of cyclin A2–Cdk2AF

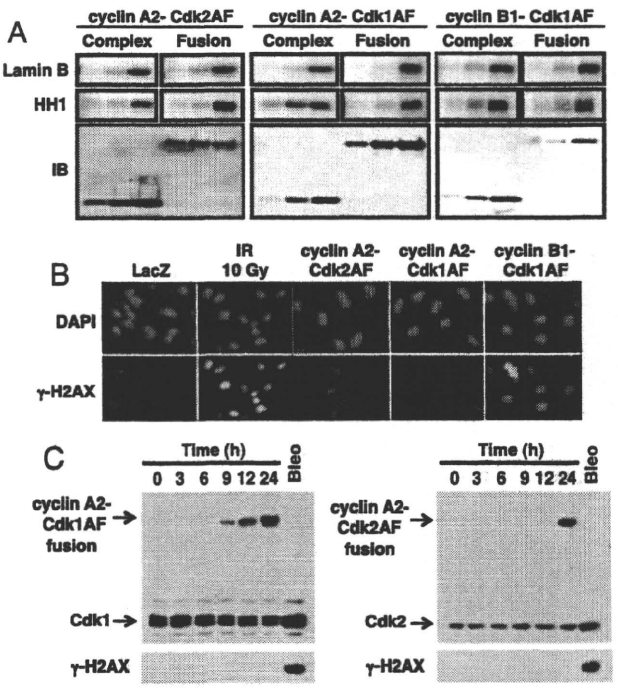

Fig. 2. Enzymatic kinetics of cyclin–Cdk fusion proteins. (*A*) Baculoviruses expressing cyclin A2 together with those expressing Cdk2 or Cdk1 (Complex) or those expressing cyclin A2–Cdk2, cyclin A2–Cdk1, or cyclin B1–Cdk1 fusion protein (Fusion) were used to infect insect cells. Their complexes or fusion proteins were purified and subjected to an in vitro kinase assay using lamin B (2 μg) or HH1 (2 μg) as a substrate or subjected to immunoblotting by using Cdk2 or Cdk1 antibodies (IB). (*B*) HeLa cells were infected with adenoviruses expressing the indicated proteins 24 h before fixing and immunostained with α-γH2AX antibodies. Their nuclei were counterstained with DAPI. As a positive control, cells infected with adenoviruses expressing LacZ were treated with IR (10 Gy). (Magnifications: 100×.) (*C*) HeLa cells were infected with adenoviruses expressing either cyclin A2-Cdk1AF or cyclin A2-Cdk2AF fusion proteins. Cells were harvested at the indicated times, and the lysates were subjected to immunoblotting using α-Cdk1 (*Upper Left*), α-Cdk2 (*Upper Right*), or α-γH2AX antibodies (*Lower*). As a control, HeLa cells were treated with bleomycin for 24 h (20 μg/mL).

did not (113.0 kb on average)(Fig. 3*C Top* and Fig. S6). Unlike Chk1 depletion, expression of cyclin A2–Cdk2AF did not cause significant changes in the proportion of abnormal replication structures (Fig. 3*C Bottom*). Taken together, these results suggested that cyclin A2–Cdk1 had a specific role in the origin firing program.

ChIP analysis revealed that considerable enrichment of early- and late-replicating DNA was specifically observed in the early and late S-phase fractions of control LacZ cells, respectively (Fig. 3*D*). Ectopic expression of cyclin A2–Cdk1AF resulted in the dramatic increase in replication of late origins in early S-phase fractions, but that of cyclin A2–Cdk2AF did not apparently affect it.

Cdk1 Is Required for Proper Timing of Origin Firing. FT210 cells possess a temperature-sensitive Cdk1 gene product (22). FACS analysis revealed a 2-h-longer S phase in FT210 cells compared with the parental FM3A cells (Fig. 4*A*). S-phase progression of FT210 cells at a permissive temperature was almost the same as that of FM3A cells. The progression of the spatiotemporal pattern of DNA replication sites in FM3A at the nonpermissive temperature was almost the same as in HeLa cells or MEFs. In contrast, the specific pattern of DNA replication sites observed in late S phase showing a few large internal foci was hardly detected in FT210 cells even at late S phase at nonpermissive temperature (Fig. 4*A*). Loss of Cdk1

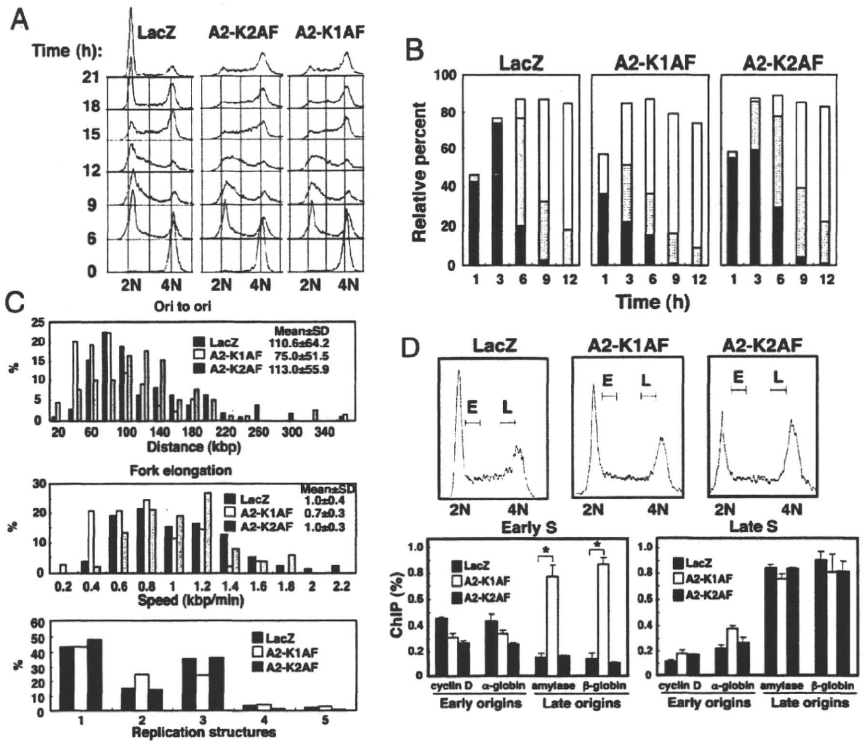

Fig. 3. Ectopic expression of cyclin A2-Cdk1AF, but not cyclin A2–Cdk2AF resulted in an aberrant temporal regulation of origin firing. (*A*) HeLa cells were synchronized by thymidine (2 mM, 24 h)/release period (6 h)/nocodazole (0.1 μg/mL, 12 h) and infected with adenoviruses expressing either cyclin A2–Cdk2AF, cyclin A2–Cdk1AF, or LacZ (control) 12 h before nocodazole washout (time 0). Cells were harvested at the indicated times, and their cell cycle profiles were analyzed by FACS. (*B*) HeLa cells were infected with the indicated adenoviruses 24 h before mimosine (0.6 mM, 16 h) washout (time 0). Replication sites were pulse-labeled for 15 min with IdU (100 μM) and then for 15 min with CldU (100 μM) before harvesting at the indicated times. The number of replication sites of each pattern was counted, and the relative percentage of the total number of cells ($n > 300$) is indicated. Black bars represent the early pattern, gray bars represent the middle pattern, and white bars represent the late pattern. Data are means of at least 3 independent experiments. (*C*) Asynchronous HeLa cells were infected with the indicated adenoviruses. Cells were harvested 24 h after infection and subjected to molecular combing. Adjacent origins in replicon clusters (Ori to ori), fork elongation, and replication structure were determined ($n > 100$) as in Fig. 1*C*. (*D*) Asynchronous HeLa cells infected with the indicated adenoviruses were pulse-labeled with BrdU before harvesting cells 24 h after infection. S-phase cells were then sorted into early (E) or late (L) fractions (*Upper*). The sorted cells were collected, and replication firing at the indicated origins was analyzed by ChIP analysis (*Lower*) as in Fig. 1*D*. Data are means ± SD of at least 3 independent experiments. Statistical significance was assessed by Student's *t* test (*, $P < 0.01$).

resulted in a significant increase in origin spacing (104.7 kb on average) when compared with control cells (78.6 kb on average) (Fig. 4*B Top* and Fig. S6). Loss of Cdk1 did not cause changes in the proportion of replication structures, further supporting the notion that Cdk1 is not involved in the stabilization of replication forks.

ChIP analysis revealed that replication patterns of early S-phase fractions in both cells were very similar, whereas replication of late origins in late S-phase fraction from FT210 cells was specifically impaired (Fig. 5*A Right*). Cdk2 activity during S phase in FT210 cells appeared the same as that in FM3A cells (Fig. S7). Collectively, these results suggested that Cdk1 activity is involved in the proper timing of late origin firing.

Finally, we attempted to determine the molecular basis by which cyclin A2–Cdk1 regulates origin firing program. In *Xenopus* and yeast systems, it was reported that cyclins, Cdk1 specifically, interact with the origin recognition complexes (ORCs) (23, 24). To examine whether the specific interaction of Cdk1 to ORCs is conserved among mammals, we performed ChIP analysis with α-Cdk1 and α-Cdk2 antibodies. Both Cdk1 and Cdk2 were detected at genes replicating early, whereas Cdk1 was specifically detected at genes replicating late (Fig. 5*B*). Relative binding of Cdk1 and Cdk2 appeared somewhat low, presumably because of an asynchronous cell cycle. These results suggested that the specific binding of Cdk1 to late origins may also be involved in the regulation of origin firing programs.

Discussion

Conditional Chk1 knockout MEFs revealed that Chk1 plays an important role in the regulation of origin firing at 2 distinct levels in mammals, namely activation of origins within a single replication factory and activation of replicon clusters (Fig. 1 *A–D*). Consistent with our observations, it was very recently proposed that Chk1 suppresses initiation in both inactive, later-firing clusters and active clusters, and the former is more strongly repressed (25). We then successfully showed that expression of cyclinA2–Cdk1AF fusion proteins activated origin firing at both levels as Chk1 depletion did (Fig. 3 *B–D*). The expression patterns of Cdk1 and cyclins during S phase and the enhancement of their activities in response to Chk1 depletion are also consistent with our conclusions (Fig. 1 *E* and *F*). The most striking evidence for the involvement of Cdk1 in DNA replication is the fact that inactivation of Cdk1 in mammalian cells resulted in a prolonged S phase accompanied by ineffective firing of late replicon clusters and reduced the density of active origins (Figs. 4 and 5*A*). Although our present results clearly demonstrate that cyclin A2–Cdk1 is involved in the regulation of late origin firing, functioning downstream of Chk1, we cannot rule out the possibility that cyclin A2–Cdk2 has a redundant function. Hochegger *et al.* (26) reported that Cdk1 activity was essential for DNA replication initiation when Cdk2 was depleted in chicken DT40 cells. When Cdk2 was present, Cdk1 inhibition did not delay S phase or block centrosome duplication. In this regard, DNA replication in DT40 cells appears complete within a shorter period (8 h) when compared with mammalian cells (10 h at 37 °C). Therefore, it is possible that DT40 cells possess a strong Cdk2 activity, presumably because of a loss of functional p53 that reduces the level of p21 Cdk inhibitor, and the high Cdk2 activity may compensate for the loss of Cdk1 activity in the context of S-phase control. In agreement with this notion, both Cdk1 and Cdk2 were recently reported to be involved in the control of DNA replication and replication origin firing under unperturbed S phase in the *Xenopus* system (27). It was also suggested that Cdk1 and Cdk2 must have different activities toward the genuine substrates involved in DNA replication although one kinase alone is minimally sufficient to promote substantial DNA replication.

Neither cyclin A2–Cdk1 nor cyclin A2–Cdk2 appeared to be involved in the stabilization of replication forks during S phase

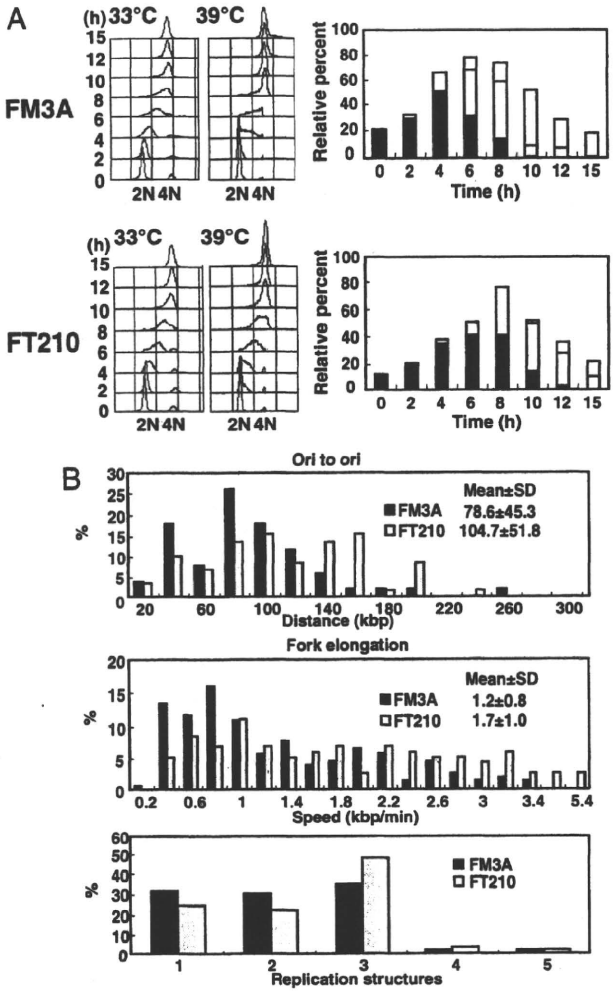

Fig. 4. Prolonged S phase in temperature-sensitive Cdk1 mutant FT210 cells. (*A*) FT210 and the parental FM3A cells were synchronized at M phase by nocodazole (0.5 μg/mL, 16 h) and then released at an either permissive (33 °C) or nonpermissive (39 °C) temperatures. Cells were then harvested 3 h after release (time 0) and at various times thereafter. Their replication sites were analyzed ($n > 300$) as in Fig. 3*B*. Data are means of at least 3 independent experiments. (*B*) Asynchronized FM3A and FT210 cells were shifted at 39 °C for 4 h. Cells were then harvested and subjected to molecular combing. Adjacent origins in replicon clusters (Ori to ori), fork elongation, and replication structure were determined ($n > 100$) as in Fig. 1C.

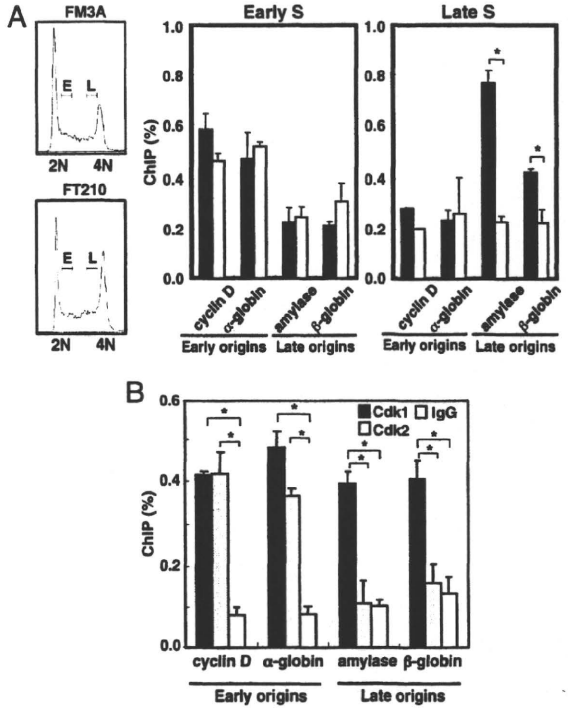

Fig. 5. Impaired late origin firing in temperature-sensitive Cdk1 mutant FT210 cells. (*A*) Asynchronous FM3A and FT210 cells were shifted at 39 °C for 4 h. Cells were pulse-labeled with BrdU (25 μM) for 1 h and sorted into early (E) or late (L) fractions. Replication firing at the indicated origins was analyzed by ChIP analysis as in Fig. 3*D*. Data are means ± SD of at least 3 independent experiments. Statistical significance was assessed by Student's *t* test (*, $P <$ 0.01). Filled bars indicate FM3A cells; empty bars indicate FT210 cells. (*B*) Asynchronous FM3A cells were cultured at 33 °C and harvested. Cell lysates were subjected to ChIP analysis as described in *Materials and Methods*. Data are means ± SD of at least 3 independent experiments. Statistical significance was assessed by Student's *t* test (*, $P < 0.01$).

when replication structures were assessed by dynamic molecular combing technology (Fig. 3*C*). This idea was further supported by the observations that ectopic expression of cyclin A2–Cdk1AF and cyclin A2–Cdk2AF failed to induce DNA damage (Fig. 2 *B* and *C*). These findings present a clear contrast to the case with Chk1 depletion in which stability of replication forks during S phase was strikingly reduced. Therefore, Chk1 likely regulates the fork stability in a manner independent of cyclin–Cdk activities.

Cdk activities have both positive and negative roles during S phase, namely to initiate DNA synthesis and prevent rereplication. A quantitative model has proposed for explain the biphasic effects of Cdks (28). In addition to a quantitative model, the accessibility of Cdk to substrates could play a role in the regulation of the S-phase program. Studies in *Xenopus* and yeast systems suggested that Cdk1 specifically interacts with ORC and phosphorylates the components more efficiently than Cdk2 although this interaction is proposed to be involved in prevention of rereplication (23, 24). We found that Cdk1 could bind to both early and late origins but Cdk2 failed to bind to late origins (Fig. 5*B*). Thus, Cdk1 could potentially activate early origin firing. This notion is supported by the fact that Cdk1 could complement the Cdk2 function of S-phase initiation in Cdk2-depleted cells (26). However, because neither ectopic expression of cyclin A2–Cdk2AF nor cyclin A2–Cdk1AF resulted in the further enhancement of early origin activation (Fig. 3*D*), activation of endogenous cyclin A/E–Cdk2 at the S-phase onset appeared to be sufficient for early origin firing. Furthermore, given that the majority of endogenous Cdk1 and Cdk2 existed in soluble fractions (Fig. S8), the origin activation program appeared to be regulated not only by induction of Cdks and their binding to prereplicative complex components, but also by alternative ways such as complex formation with cyclins or regulation of inhibitory phosphorylation of Cdks. In this regard, it was very recently reported that Cdk1 started to form a complex with cyclin A2 after cyclin A2–Cdk2 complexes reached a plateau in mid S phase (21). Taken together, our results suggest that cyclin A2–Cdk1 may regulate origin firing program through both its specific accessibility to late origins and regulation of Cdk1 activity at late S phase.

In conclusion, the present results indicate that ATR/Chk1–cyclin A2–Cdk1 controls the activation of late replication origins and the density of active origins in mammals. Similar regulation was reported in a budding yeast system in which Clb5–Cdk1 was required for late origin firing (8). Taken together, these results suggest the existence of conserved mechanisms for the temporal program of origin activation among a number of eukaryotes.

Materials and Methods

Antibodies. Antibodies used in this study were as follows: α-CDK2 (sc-748; Santa Cruz), α-Cyclin A2 (sc-751; Santa Cruz), α-Cdc2 (sc-54; Santa Cruz), α-Cyclin B1 (sc-245; Santa Cruz), rat α-BrdU (ab6326; Abcam), mouse α-BrdU (347580; BD), α-γH2AX (05-636; Upstate), α-rabbit IgG HRP (NA934; GE Healthcare), α-mouse IgG HRP (NA931; GE Healthcare), Alexa Fluor 555-conjugated goat α-mouse IgG (A-21422; Invitrogen), and Alexa Fluor 488-conjugated rabbit α-rat IgG (A-21210; Invitrogen).

Cell Culture and Double Labeling with IdU and CldU. HeLa cells, Chk1$^{lox/-}$ MEFs, Chk1$^{del/-}$ MEFs, FM3A, and FT210 cells were cultured as described (14, 29). For analyses of origin firing programs, cells were incubated with 100 μM IdU for 15 min, then 100 μM CldU for 15 min, fixed with 4% paraformaldehyde, and permabilized. Cellular DNA was denatured in 1.5 M HCl and stained as reported (6). The spatiotemporal patterns of replication were analyzed by counting at least 300 cells by 2 individuals under blinded conditions.

Dynamic Molecular Combing and Immunofluorescent Detection. Genomic DNA was prepared and combed onto the silanated cover slips as described (30) with modifications as detailed (31). A total of 2×10^6 cells were pulse-labeled for 20 min with 100 μM IdU, washed with PBS twice, and pulse-labeled for 20 min with 100 μM CldU. For preparation of genomic DNA, to remove the mitochondrial genome the nuclei were extracted with buffer A [250 mM sucrose, 20 mM Hepes (pH 7.5), 10 mM KCl, 1.5 mM $MgCl_2$, 1 mM EDTA (pH 8.0), 1 mM EGTA (pH 6.8), 1 mM DTT, 0.1 mM PMSF] before resuspension into low-melting point agarose. Combed DNA molecules were heat-denatured in 50% formamide, 2 × SSC at 72 °C for 12 min. For immunodetection of labeled DNA, denatured DNA molecules were incubated with mouse α-BrdU mAb (1:5) and rat α-BrdU mAb (1:25) for 1 h at 37°C. After washing with PBS and 0.05% Tween 20 for 5 min 3 times, DNA molecules were incubated with Alexa Fluor 555-conjugated goat α-mouse IgG (1:500) and Alexa Fluor 488-conjugated rabbit α-rat IgG (1:500) for 30 min at 37°C. All antibodies were diluted in blocking solution [1% (wt/vol) blocking reagent in PBS, 0.05% Tween 20]. After washing with PBS and 0.05% Tween 20 for 5 min 3 times, coverslips were mounted in VECTASHIELD (Vector Laboratories). To estimate the extension of DNA molecules, coverslips were prepared with λ-DNA, and then the DNA molecules were stained with 6.7 mM YOYO-1 at 25°C for 1 h. YOYO-1-stained DNA molecules measured 21 ± 0.9 μm. As the virus genome is 48.5 kbp, the extension of DNA molecules is 2.32 ± 0.11 kbp/μm. DNA fibers were examined with a Zeiss Axioplan 2 MOT with a 63X Plan-APOCHROMAT (NA 1.4) objective lens, equipped with MicroMAX CCD camera (Princeton Instruments). Fluorescent signals were measured by using MetaMorph version 6.1 software (Universal Imaging).

Construction of Cyclin A2–Cdk1, Cyclin A2–Cdk2, and Cyclin B1–Cdk1 Fusion Vectors. For subcloning of full-length mouse Cdk1 and Cdk1AF, either cDNAs from mouse MEFs or pcDNA3.1Cdk1AF were used as a template. The PCR products were digested with EcoRI and NotI and subcloned into pcDNA3.1Myc/HisA vector (Invitrogen). For subcloning of full-length mouse Cdk2 and Cdk2AF, either cDNAs from mouse MEFs or pcDNA3.1Cdk2AF were used as a template. For preparation of cyclin A2–Cdk1, cyclin A2–Cdk2, and cyclin B1–Cdk1 fusion constructs, sets of primers and mouse cDNA derived from MEFs as a template were used. The PCR products were digested with BamHI and EcoRI and subcloned into pcDNA3.1Cdk1Myc/HisA or pcDNA3.1Cdk2Myc/HisA vectors. The primer sets used are listed in Table S1.

Purification of Recombinant Cyclin–Cdk Fusion Proteins. pcDNA3.1cyclin A2–Cdk1, pcDNA3.1cyclin A2–Cdk2, pcDNA3.1cyclin B1–Cdk1, and their AF mutants were digested with BamHI and PmeI. The fragments were subcloned into pVL1392 vector and transfected into Sf9 cells. Sf9 cells infected with baculoviruses expressing cyclin–Cdk fusion proteins or coinfected with the individual cyclins and Cdks were lysed with immunoprecipitation kinase buffer (7) containing a mixture of protease inhibitors. The fusion proteins and cyclin–Cdk complexes were purified by ProBond Resin (Invitrogen) and used for the in vitro kinase assay.

Preparation of Adenoviruses Expressing Cyclin–Cdk Fusion Proteins. The BamHI–PmeI fragments of cyclin–Cdk fusion constructs were subcloned into pENTER vector (Invitrogen) predigested with BamHI and EcoRV. pENTERcyclin–Cdks and pENTERcyclin–CdkAFs were then subcloned into pAdCMV vectors according to the manufacturer's instructions (Invitrogen). pAdcyclin–Cdks and pAdcyclin–CdkAFs were transfected into 293A cells (Invitrogen).

ChIP Assay. Asynchronized Chk1$^{lox/-}$ MEFs, Chk1$^{del/-}$ MEFs, HeLa cells infected with adenoviruses expressing cyclin A2–Cdk1AF or cyclin A2–Cdk2AF, and mouse FM3A or FT210 cells were labeled with 25 μM BrdU before cell sorting. Cells were then sorted into early and late S-phase fractions by using a cell sorter (BD). At least 60,000 cells were collected during each phase and used for the chromatin preparation. Nascent DNA was enriched by immunoprecipitation using α-BrdU antibodies as reported (16) and subjected to quantitative PCR with the ABI PRISM7000 system using Power SYBR Green PCR Master Mix (Applied Biosystems). Primers used for PCR are listed in Table S1. As a control, mtDNA in BrdU-containing DNA was also amplified, and the results were presented as a percentage of mtDNA. For Cdk1 and Cdk2 bindings to origins, FM3A cells were cultured at 33 °C, and ChIP analysis was performed with α-Cdk1 and α-Cdk2 antibodies as described (14). The results were presented as a percentage of input.

ACKNOWLEDGMENTS. We thank Dr. C. Namikawa-Yamada, Mr. K. Murata, and Miss H. Kojima for technical assistance. This work was supported in part by the Ministry of Education, Science, Sports, and Culture of Japan through a Grant-in-Aid of Scientific Research (to M.N.).

1. Machida YJ, Hamlin JL, Dutta A (2005) Right place, right time, and only once: Replication. *Cell* 123:13–24.
2. Jackson DA (1995) Nuclear organization: Uniting replication foci, chromatin domains, and chromosome structure. *BioEssays* 17:587–591.
3. Woodward AM, *et al.* (2006) Excess Mcm2–7 license dormant origins of replication that can be used under conditions of replicative stress. *J Cell Biol* 173:673–683.
4. Shechter D, Gautier J (2005) ATM and ATR check in on origins: A dynamic model for origin selection and activation. *Cell Cycle* 4:235–238.
5. Shechter D, Costanzo V, Gautier J (2004) ATR and ATM regulate the timing of DNA replication origin firing. *Nat Cell Biol* 6:648–655.
6. Maya-Mendoza A, Petermann E, Gillespie DA, Caldecott KW, Jackson DA (2007) Chk1 regulates the density of active replication origins during the vertebrate S phase. *EMBO J* 26:2719–2731.
7. Niida H, *et al.* (2005) Depletion of Chk1 leads to premature activation of Cdc2-cyclin B and mitotic catastrophe. *J Biol Chem* 280:39246–39252.
8. Donaldson AD, *et al.* (1998) CLB5-dependent activation of late replication origins in *S. cerevisiae*. *Mol Cell* 2:173–182.
9. Heichinger C, Penkett CJ, Bahler J, Nurse P (2006) Genomewide characterization of fission yeast DNA replication origins. *EMBO J* 25:5171–5179.
10. Dai J, Chuang RY, Kelly TJ (2005) DNA replication origins in the *Schizosaccharomyces pombe* genome. *Proc Natl Acad Sci USA* 102:337–342.
11. Patel PK, Arcangioli B, Baker SP, Bensimon A, Rhind N (2006) DNA replication origins fire stochastically in fission yeast. *Mol Biol Cell* 17:308–316.
12. Jeon Y, *et al.* (2005) Temporal profile of replication of human chromosomes. *Proc Natl Acad Sci USA* 102:6419–6424.
13. Sadoni N, Cardoso MC, Stelzer EH, Leonhardt H, Zink D (2004) Stable chromosomal units determine the spatial and temporal organization of DNA replication. *J Cell Sci* 117:5353–5365.
14. Shimada M, *et al.* (2008) Chk1 is a histone H3 threonine 11 kinase that regulates DNA damage-induced transcriptional repression. *Cell* 132:221–232.
15. O'Keefe RT, Henderson SC, Spector DL (1992) Dynamic organization of DNA replication in mammalian cell nuclei: Spatially and temporally defined replication of chromosome-specific α-satellite DNA sequences. *J Cell Biol* 116:1095–1110.
16. Hiratani I, Leskovar A, Gilbert DM (2004) Differentiation-induced replication-timing changes are restricted to AT-rich/long interspersed nuclear element (LINE)-rich isochores. *Proc Natl Acad Sci USA* 101:16861–16866.
17. Aladjem MI, *et al.* (2002) Replication initiation patterns in the β-globin loci of totipotent and differentiated murine cells: Evidence for multiple initiation regions. *Mol Cell Biol* 22:442–452.
18. Jiang K, *et al.* (2003) Regulation of Chk1 includes chromatin association and 14–3-3 binding following phosphorylation on Ser-345. *J Biol Chem* 278:25207–25217.
19. Niida H, Katsuno Y, Banerjee B, Hande MP, Nakanishi M (2007) Specific role of Chk1 phosphorylations in cell survival and checkpoint activation. *Mol Cell Biol* 27:2572–2581.
20. Bartek J, Lukas J (2003) Chk1 and Chk2 kinases in checkpoint control and cancer. *Cancer Cell* 3:421–429.
21. Merrick KA, *et al.* (2008) Distinct activation pathways confer cyclin-binding specificity on cdk1 and cdk2 in human cells. *Mol Cell* 32:662–672.
22. Th'ng JP, *et al.* (1990) The FT210 cell line is a mouse G_2 phase mutant with a temperature-sensitive CDC2 gene product. *Cell* 63:313–324.
23. Romanowski P, *et al.* (2000) Interaction of *Xenopus* Cdc2 × cyclin A1 with the origin recognition complex. *J Biol Chem* 275:4239–4243.
24. Wuarin J, Buck V, Nurse P, Millar JB (2002) Stable association of mitotic cyclin B/Cdc2 to replication origins prevents endoreduplication. *Cell* 111:419–431.
25. Ge XQ, Jackson DA, Blow JJ (2007) Dormant origins licensed by excess Mcm2–7 are required for human cells to survive replicative stress. *Genes Dev* 21:3331–3341.
26. Hochegger H, *et al.* (2007) An essential role for Cdk1 in S phase control is revealed via chemical genetics in vertebrate cells. *J Cell Biol* 178:257–268.
27. Krasinska L, *et al.* (2008) Cdk1 and Cdk2 activity levels determine the efficiency of replication origin firing in *Xenopus*. *EMBO J* 27:758–769.
28. Porter AC (2008) Preventing DNA overreplication: A Cdk perspective. *Cell Div* 3:3.
29. Fujita M, *et al.* (1998) Cell cycle- and chromatin binding state-dependent phosphorylation of human MCM heterohexameric complexes: A role for cdc2 kinase. *J Biol Chem* 273:17095–17101.
30. Michalet X, *et al.* (1997) Dynamic molecular combing: Stretching the whole human genome for high-resolution studies. *Science* 277:1518–1523.
31. Sugimura K, Takebayashi S, Taguchi H, Takeda S, Okumura K (2008) PARP-1 ensures regulation of replication fork progression by homologous recombination on damaged DNA. *J Cell Biol* 183:1203–1212.

ELSEVIER

Cancer Detection and Prevention xxx (2008) xxx–xxx

Cancer Detection and Prevention

www.elsevier.com/locate/cdp

Peroxisome proliferator-activated receptor-γ and growth inhibition by its ligands in prostate cancer

Daisuke Nagata MD[a], Yoshihiro Hashimoto MD, PhD[a,*], Makoto Nakanishi MD, PhD[b], Hiromichi Naruyama MD[a], Shinsuke Okada MD[a], Ryosuke Ando MD[a], Keiichi Tozawa MD, PhD[a], Kenjiro Kohri MD, PhD[a]

[a] *Department of Nephro-urology, Nagoya City University Graduate School of Medical Sciences, 1 Kawasumi, Mizuho-cho, Mizuho-ku, Nagoya, Japan*
[b] *Department of Biochemistry and Cell Biology, Nagoya City University Graduate School of Medical Sciences, 1 Kawasumi, Mizuho-cho, Mizuho-ku, Nagoya, Japan*

Accepted 30 May 2008

Abstract

Background: Peroxisome proliferator-activated receptor-γ (PPAR-γ) is expressed in certain human cancers. Ligand-induced PPAR-γ activation can result in growth inhibition and differentiation in these cancer cells; however, the precise mechanism for the anti-proliferative effect of PPAR-γ ligands is not clear. *Methods*: In this study, we examined the expression of PPAR-γ in human prostate cancer and the effect of two PPAR-γ ligands, 15 deoxy-$\Delta^{12,14}$-prostaglandin J2 (15d-PGJ2) and troglitazone, on prostate cancer cell growth. *Results*: PPAR-γ is frequently over-expressed in androgen independent prostate cancer cell lines and human prostate cancer tissues (22 of 47; 47%). Both 15d-PGJ2 and troglitazone inhibited proliferation and DNA synthesis of prostate cancer cell lines in a dose-dependent manner, and slightly increased the proportion of cells with S-phase DNA content. Prostate specific antigen (PSA) promoter reporter assays showed that troglitazone and 15d-PGJ2 down-regulated androgen stimulated reporter gene activity in prostate cancer cell lines LNCaP. Interestingly, LNCaP with troglitazone dramatically suppressed PSA protein expression without suppressing AR expression. *Conclusions*: Taken together, these results suggest that PPAR-γ ligands may be a useful therapeutic agent for the treatment of prostate cancer.

Keywords: PPAR-γ; Ligand; Prostate cancer

1. Introduction

Prostate cancer is the most common cancer among men and the second leading cause of male cancer death [1]. Although surgical resection or radiotherapy is potentially curative for localized disease, advanced prostate cancer is associated with a poor prognosis. Conventional chemotherapy and radiotherapy are of limited effectiveness. Blockade of androgen stimulation often leads to either a partial or full remission; however, subsequent relapse often occurs and the disease re-emerges within a few years in a poorly differentiated, androgen-independent form. The shortage of curative therapies for advanced disease has provided impetus for the development of novel therapies.

Peroxisome proliferator-activated receptor (PPAR) is a member of the steroid hormone receptor superfamily involved in ligand-inducible regulation [2–5]. There are three types of PPARs: PPAR-α, PPAR-β, and PPAR-γ. All PPAR isoforms require heterodimerization with the retinoid X receptor for optimal DNA binding and transcriptional activity [6].

PPAR-γ is an important molecule for adipocyte differentiation and is over-expressed in adipose tissue [7,8]. In addition to adipose tissue, PPAR-γ expression is

Abbreviations: 15d-PGJ2, 15-deoxy-$\Delta^{12,14}$-prostaglandin J2; AR, androgen receptor; DHT, 5alpha-dihydrotestosterone; FACS, fluorescence-activated cell sorter; PPAR, peroxisome proliferator-activated receptor; PSA, prostate specific antigen.

* Corresponding author. Tel.: +81 52 853 8266; fax: +81 52 852 3179.
E-mail address: hashi@med.nagoya-cu.ac.jp (H. Yoshihiro).

0361-090X/$30.00
doi:10.1016/j.cdp.2008.05.008

Please cite this article in press as: Nagata D, et al. Peroxisome proliferator-activated receptor-γ and growth inhibition by its ligands in prostate cancer, Cancer Detect Prev (2008), doi:10.1016/j.cdp.2008.05.008

detected in a wide variety of cancer cells [9–13]. The receptor requires ligand activation, and several ligands have been identified including synthetic antidiabetic thiazolidinedione (TZD) drugs and natural ligands such as 15d-PGJ2 [14]. Troglitazone is a TZD that has been widely used for insulin-resistant diabetes mellitus, and has been identified as a specific ligand for PPAR-γ [15–17]. In cancer cells, PPAR-γ activation by its high affinity ligands can inhibit cell proliferation [18,19]. Thus PPAR-γ is involved in not only lipid metabolism but also cellular proliferation in cancer cells. Therefore, it is suggested that PPAR-γ is a possible molecular target for cancer treatment. Although increasing evidence has established that PPAR-γ activation induces growth arrest in cancer cells, the molecular mechanism of the growth inhibition by PPAR-γ ligands is not well understood. Some researchers have recently demonstrated that the cyclin-dependent kinase inhibitor may be a crucial molecule in the cell growth inhibition by PPAR-γ ligands in human cancer cells [18–21]. In this study, we show that PPAR-γ is expressed in human prostate cancer, and that ligand activation of this nuclear hormone receptor inhibits prostate cancer cell proliferation and activity of androgen-responsive gene, such as prostate specific antigen (PSA).

2. Materials and methods

2.1. Cells and samples

Prostate cancer cell lines (LNCaP, PC-3, and DU145) were obtained from the American Type Culture Collection (Rockville, MD). PC-3 and DU145 were maintained in Dulbecco's modified eagle's media (DMEM) with 10% FCS. LNCaP was grown in RPMI1640 with 10% FCS. 15-deoxy-$\Delta^{12,14}$-prostaglandin J2 (15d-PGJ2) and troglitazone (Sigma Chemical Co.; St. Louis, MO) were dissolved in a solution containing 50% dimethyl sulfoxide (DMSO) and 50% ethanol and applied to cells at a concentration of <0.1% of the media volume. Prostate cancer tissue and adjacent normal prostate tissue ($n = 47$) were surgically obtained after informed consent from patients, and were fixed by a standard method for immunohistochemistry.

2.2. Cell growth assay (cell viability assay)

For experiments, each prostate cancer cell line was plated at a density of 2×10^3 cm^{-2}. One day later (at day 0), the medium was changed to the maintenance medium with 15d-PGJ2 or troglitazone. Adherent cells were harvested by trypsinization and collected by centrifugation. Nonadherent cells were collected from spent media by centrifugation. Cell pellets were resuspended in 100 μl of fresh media, and trypan blue solution (Sigma) was added at a ratio of 1:1. Viable cells were counted by trypan blue exclusion using a hemocytometer as a percentage of a total of 500 cells. Each experiment was carried out in quadruplicate and repeated at least three times.

2.3. Cell cycle analysis

After treatment with ligands at varying concentrations (described in Table 2), cells were washed with chilled phosphate-buffered saline (PBS) and kept on ice in phosphate-buffered saline containing 2 mM ethylenediaminetetraacetate (EDTA) (Sigma Chemical Co.) for 10 min. Cells were collected using a cell scraper, suspended in PBS, and fixed with 0.25% paraformaldehyde (Sigma Chemical Co.). Fixed cells were washed once with PBS, incubated with 100 mg of RNase A (Sigma Chemical Co.) in PBS containing 0.2% Tween 20, and stained with 50 mg/ml of propidium iodide (Sigma Chemical Co.). Cell cycle analysis was performed with a fluorescence-activated cell sorter (FACS) Calibur flow cytometer (Becton Dickinson, Mansfield, MA). The percentage of cells in the G0/G1, S and G2/M phases of the cell cycle was determined using the Modfit LT software program (Verity Software House Inc., Topsham, ME).

2.4. DNA synthesis inhibitory assay

Cell proliferation was determined by measurement of tritiated thymidine incorporation during DNA synthesis via a radioactive assay as described previously [22]. All cells were treated with 0, 2.5, and 10 μM 15d-PGJ2 or 0, 5, and 20 μM toglitazone for 24 h. Additionally these cells were incubated with tritiated thymidine (1 mCi/ml) solution for 24 h prior to harvesting.

2.5. Western blot analysis

Total cell lysates were prepared by boiling cells in sodium dodecylsulfate (SDS) sample buffer after treatment with 15d-PGJ2 and troglitazone. Samples were equalized to 20 μg/lane and run on a 12% SDS-polyacrylamide gel. Proteins were transferred to nitrocellulose membranes (Bio-Rad). Blocked membranes were incubated overnight with either anti-PPAR-γ polyclonal antibody (Santa Cruz; 1:2000 dilution), anti-AR polyclonal antibody (Santa Cruz; 1:500 dilution), anti-PSA polyclonal antibody (Santa Cruz; 1:500 dilution), or anti-β-actin polyclonal antibody (Santa Cruz; 1:500 dilution). Three 10-min washes in Tris-buffered saline (TBS)-Tween 20 (20 mM Tris–HCl, 137 mM NaCl, and 0.1% Tween 20, pH 7.6) were carried out between antibody steps, followed by incubation with antirabbit secondary antibody conjugated to horseradish peroxidase (Amersham; 1:2000 dilution) for 1 h at room temperature. The signals were detected by enhanced chemiluminescence (Amersham). The stripping procedures were performed using standard methods.

Please cite this article in press as: Nagata D. et al., Peroxisome proliferator-activated receptor-γ and growth inhibition by its ligands in prostate cancer, Cancer Detect Prev (2008), doi:10.1016/j.cdp.2008.05.008

2.6. Immunohistochemistry

Immunohistochemical staining was performed with the Vectastatin avidin–biotin peroxidase complex kit (Vector, Burlingame, CA). Formalin-fixed, paraffin-embedded specimens were sectioned onto microscope slide at a thickness of 3 μm, and then deparaffinized in xylene and rehydrated in graded ethanol. Endogenous peroxide was blocked with 0.3% hydrogen peroxide in methanol for 30 min. Sections were reacted with the primary antibody (Santa Cruz; anti-PPAR-γ polyclonal antibody diluted at 1:500) for 24 h at 4 °C, washed with PBS, and incubated with biotinylated secondary antibody for 30 min at room temperature, followed by treatment with the avidin–biotin peroxidase complex (DAKO) for 30 min at room temperature. Sections were washed with PBS, and peroxidase activity was visualized with 0.03% 3,3′-diaminobenzidine tetrahydrochloride containing 0.06% H_2O_2 in ammonium acetate –citric buffer. Sections were counterstained with hematoxylin. For each slide, the extent and intensity of staining with PPAR-γ antibody was graded on a scale of 0–3+ by two blinded observers on two separate occasions using coded slides, and an average score was calculated.

2.7. Transfections and luciferase assay

LNCaP cells were incubated in RPMI 1640 with 10% FBS until 50–70% confluency. Cells were transfected with PSA promoter luciferase reporter gene using the Lipofectamine plus (Gibco) under serum-free conditions. A pCMV-β-galactosidase vector was included as an internal control for efficiency of transfection. Following transfections, cells were incubated in RPMI1640 with 10% charcoal-stripped fetal bovine serum FBS either with or without 10–9 M 5alpha-dihydrotestosterone (DHT) and either with or without ligands for PPAR-γ for 72 h. Cells were collected with tissue lysis buffer. Luciferase activity of the cell lysates was measured by luminometry, and activities were normalized by β-galactosidase activities. All transfection experiments were carried out in triplicate wells and repeated separately at least three times.

3. Results

3.1. Expression of PPAR-γ in prostate cancer cell lines and human prostate tissues

We initially examined the expression levels of PPAR-γ in prostate cancer cell lines using Western blot analysis (Fig. 1A). We found variable levels of PPAR-γ protein with moderate expression seen in the androgen independent cell lines, PC-3 and DU145, and low expression in the androgen-dependent cell line, LNCaP. Expression levels were corrected for differences in protein loading according to probing with antibody to β-actin. In addition, we evaluated the expression levels of PPAR-γ in human prostate tissues by immunohistochemistry. Tumor area was expressed at a significant level; in contrast, non-tumor prostate area was expressed at a very low or negligible level (Fig. 1B and Table 1).

3.2. PPAR-γ ligands inhibit proliferation of prostate cancer cells

Each prostate cancer cell line was plated at a density of 2×10^3 cm^{-2} and incubated in the maintenance medium with 15d-PGJ2 or troglitazone. The effect of each ligand on

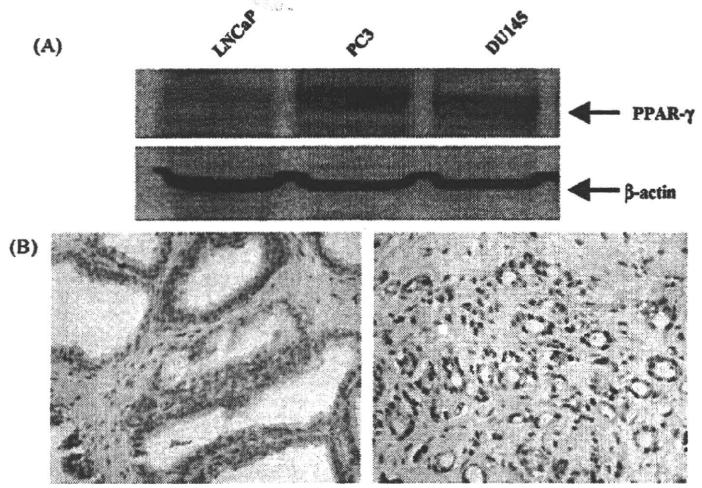

Fig. 1. Expression of PPAR-γ in prostate cancer cell lines and human prostate tissues. (A) Western blot analysis of PPAR-γ in prostate cancer cell lines Lysates were extracted from four prostate cancer cell lines. The lysates were electrophoresed, blotted on membrane, and reacted with a specific antibody to PPAR-γ. The antibody was removed from the membrane and incubated with an antibody to β-actin. Expression levels were corrected for differences in protein loading according to actin probing. (B) Immunohistochemistry for PPAR-γ in prostate cancer. Weak expression of immunoreactive PPAR-γ was found in non-tumor area (left: ×400). In contrast, we found significant expression of immunoreactive PPAR-γ in tumor area (right: ×400).

Please cite this article in press as: Nagata D, et al., Peroxisome proliferator-activated receptor-γ and growth inhibition by its ligands in prostate cancer, Cancer Detect Prev (2008), doi:10.1016/j.cdp.2008.05.008

Table 1
Immunohistochemistry of PPAR-γ in human prostate cancer patients

	Intensity			Positive (%)	Total samples
	+	++	+++		
Tumor	5	13	4	22 (46.8%)	47
Non-tumor	6	0	0	6 (12.8%)	47

Tissues were obtained from the center of grossly recognizable nodules of prostate cancer. The formalin-fixed, paraffin-embedded tissue sections were deparaffinized, rehydrated and subjected to immunohistochemistry study with anti-PPAR-γ antibody (1:200 dilution, Santa Cruz) according to standard protocols. The staining intensity was scored on a 0–3 scale from negative to strong immunoreactivity.

the growth response of the cells was determined by a cell viability assay using trypan blue. Low concentrations of troglitazone (5 μM) and 15d-PGJ2 (2.5 μM) blocked cell proliferation on all prostate cancer cell lines (Fig. 2).

3.3. PPAR-γ ligands inhibit DNA synthesis of prostate cancer cells

To confirm the effect of PPAR-γ ligands on cell proliferation, the incorporation of tritiated thymidine into DNA was measured in a radioactive DNA synthesis assay. As shown in Fig. 3, treatment with 15d-PGJ2 or troglitazone decreases DNA synthesis significantly in all prostate cancer cell lines at 24 h post-treatment.

3.4. PPAR-γ ligands treatment causes S-phase cell arrest in prostate cancer cells

Because of the profound inhibition of cellular proliferation caused by PPAR-γ ligands, we wanted to determine whether the cell cycle was altered. LNCaP, PC-3, and DU145 were treated with 10 μM 15d-PGJ2 or 20 μM troglitazone for 48 h, at which time cell cycle changes were studied by FACS analysis. These cell lines showed no significant increase in the proportion of cells in the G0–G1 phase and the apoptotic phase of cell cycle. All cell lines showed mild accumulation of cells in the S-phase at 48 h post-treatment with 15d-PGJ2 and troglitazone compared with control cells (Table 2).

3.5. PPAR-γ ligands down-regulate PSA promoter activity in LNCaP cell

To explore potential mechanisms by which PPAR-γ ligands inhibited levels of PSA as androgen-responsive gene, we analyzed the effect of 15d-PGJ2 and troglitazone on the ability of DHT to transactivate the PSA promoter. The LNCaP prostate cancer cells were cultured with DHT after being transfected with the PSA promoter luciferase reporter. The reporter activity increased about 17-fold as compared with nontreated control LNCaP cells. This result was consistent with previous observations. When cells were treated with both troglitazone and DHT, luciferase activity dramatically reduced by 65% compared with DHT alone (Fig. 4).

3.6. Effect of PPAR-γ ligands on PSA, AR, and PPAR-γ expression in LNCaP cell

Cytoplasmic PSA protein expression was studied by Western blot analyses of LNCaP cells cultured with or without troglitazone and DHT for different durations (Fig. 5). LNCaP cells constitutively expressed PSA protein, and when these cells were incubated with DHT, PSA expression increased 1.7-fold after 48 h of culture. Troglitazone suppressed PSA expression induced by DHT at each time point. For example, at day 2, troglitazone

Table 2
Cell cycle analysis of prostate cancer cell lines treated with PPAR-γ ligands

	Proportion of cells			
	G0/G1	S	G2/M	Apoptotic
LNCaP				
Control	72.23 ± 2.08	3.21 ± 0.23	24.57 ± 1.86	1.21 ± 0.13
15d-PGJ2 (10 μM)	68.37 ± 0.71	15.17 ± 0.11	16.81 ± 0.78	1.77 ± 0.35
Troglitazone (20 μM)	74.22 ± 1.74	9.47 ± 0.34	16.32 ± 0.62	0.94 ± 0.26
PC-3				
Control	54.18 ± 0.48	24.52 ± 0.18	21.31 ± 0.60	2.17 ± 0.53
15d-PGJ2 (10 μM)	47.16 ± 1.59	39.71 ± 0.58	13.14 ± 0.70	4.65 ± 1.71
Troglitazone (20 μM)	58.13 ± 2.43	31.69 ± 3.12	10.18 ± 1.08	2.93 ± 0.42
DU145				
Control	53.56 ± 1.24	17.26 ± 1.17	29.20 ± 0.12	3.52 ± 0.88
15d-PGJ2 (10 μM)	35.27 ± 4.59	44.38 ± 5.45	20.15 ± 2.33	6.46 ± 1.26
Troglitazone (20 μM)	56.14 ± 5.41	29.73 ± 1.76	14.34 ± 0.97	3.19 ± 0.79

Cells were treated with 10 μM 15d-PGJ2 or 20 μM troglitazone for 48 h. The effect of these ligands on the proportion of cells in each phase of the cell cycle was determined. Data shown is representative of three experiments. Values are mean ± S.D.

Please cite this article in press as: Nagata D, et al., Peroxisome proliferator-activated receptor-γ and growth inhibition by its ligands in prostate cancer. Cancer Detect Prev (2008), doi:10.1016/j.cdp.2008.05.008

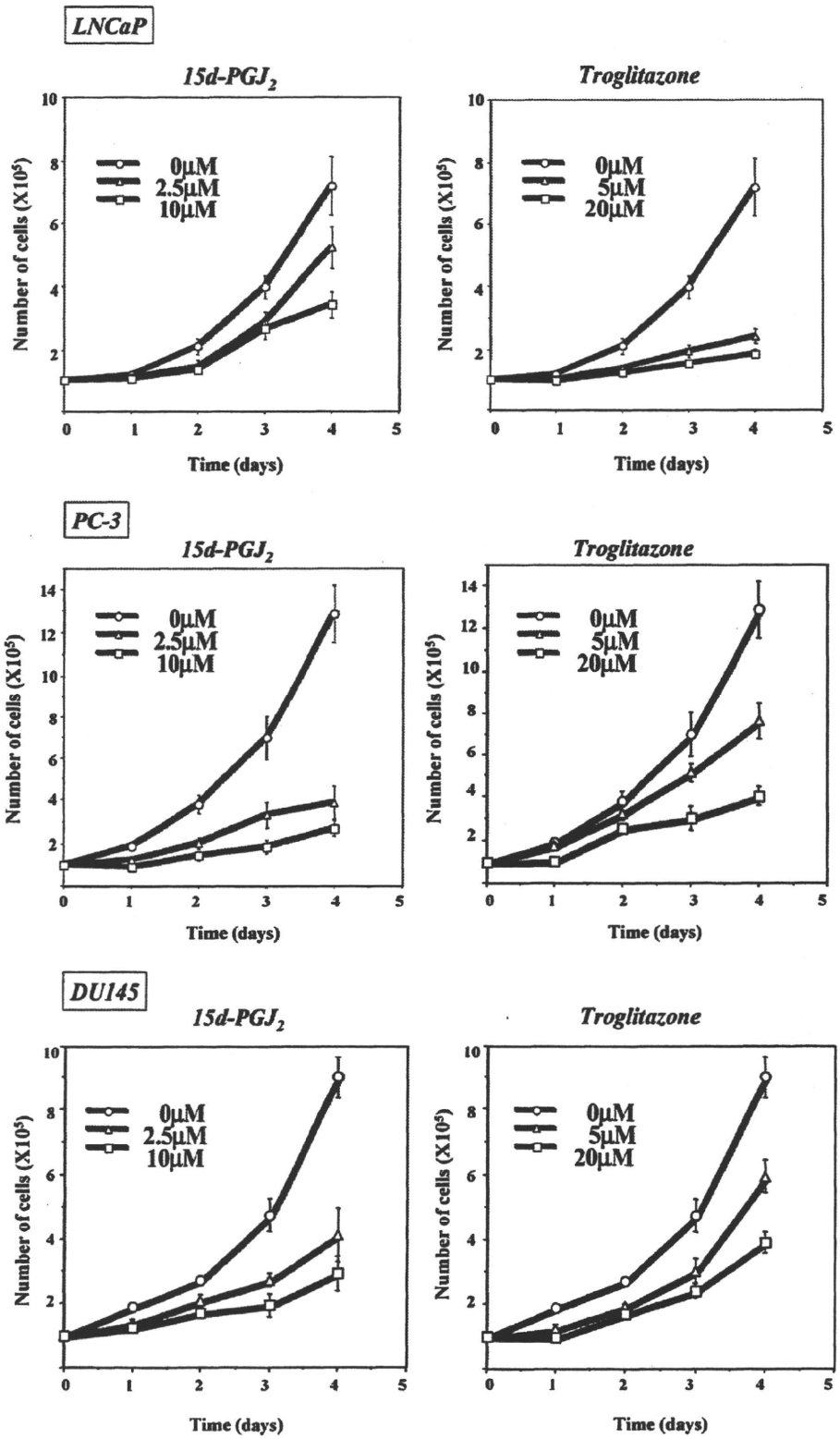

Fig. 2. Effects of PPAR-γ ligands on prostate cancer cell analyzed by cell number. After being plated at 2×10^3 cm^{-2} in the maintenance medium (described in Section 2), cells were incubated in maintenance medium with 15d-PGJ2 or troglitazone on the following day. The number of viable cells was counted by trypan blue exclusion using a hemocytometer. Data are shown as mean of the triplicate dishes.

Please cite this article in press as: Nagata D, et al., Peroxisome proliferator-activated receptor-γ and growth inhibition by its ligands in prostate cancer, Cancer Detect Prev (2008), doi:10.1016/j.cdp.2008.05.008

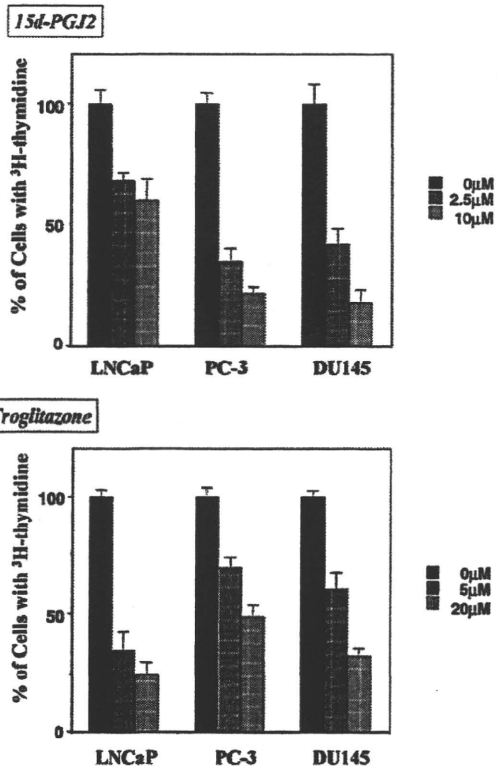

Fig. 3. Effects of PPAR-γ ligands on prostate cancer cell analyzed by DNA synthesis. LNCaP, PC-3 and DU145 were treated with 15d-PGJ2 or toglitazone for 24 h. Additionally, cells were incubated with tritiated thymidine (1 mCi/ml) solution for 24 h prior to harvesting. The amount of synthesized DNA was measured by the method described in Section 2 ($n = 3$); bars, S.D.

suppressed PSA levels by 70% as compared with cells cultured with DHT alone. Moreover, we examined levels of AR in LNCaP to determine whether troglitazone suppressed PSA through inhibition of AR expression. Troglitazone did not significantly affect levels of AR expression compared

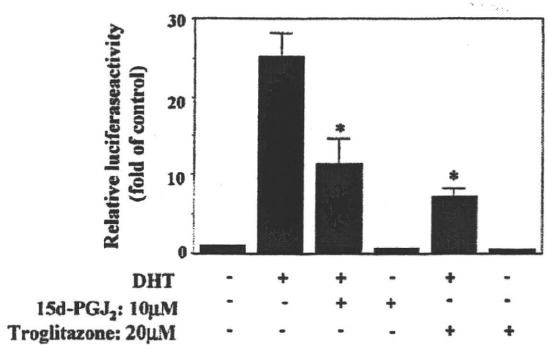

Fig. 4. Effect of PPAR-γ ligands on transcriptional activity of PSA promoter in LNCaP cells. LNCaP cells were transfected with PSA-Luc. DHT (10^{-9} M) either with or without PPAR-γ ligand (15d-PGJ2: 10 μM, troglitazone: 20 μM) was added. pCMV-β-galactosidase vector was cotransfected for normalization. S.D.s from three or more repetitions of the experiment are shown. $^{*}P < 0.05$ as determined by Student's t test difference compared with DHT alone.

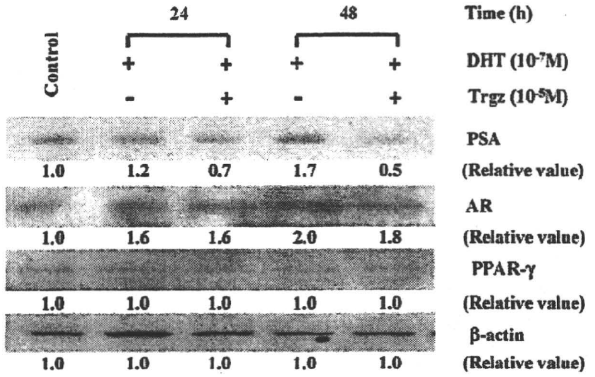

Fig. 5. Western blot analysis of PSA, AR, PPAR-γ and b-actin in LNCaP cells treated with troglitazone. Cells were incubated in medium with 10% charcoal-striped FBS for 24 h before the addition of 10^{-9} M DHT either with (+) or without (−) 10^{-5} M troglitazone. After the addition of reagents, cells were incubated for 24 and 48 h. Control: cell lysates harvested before the addition of reagents. The relative abundance of band intensity was measured by densitometric scanning.

with LNCaP cells cultured with DHT alone. Furthermore, neither DHT nor troglitazone affected levels of PPAR-γ (Fig. 5).

4. Discussion

PPAR-γ belongs to the nuclear steroid receptor superfamily, which includes receptors for steroids, thyroid hormone, retinoid acid and vitamin D. These receptors are critical for cellular growth and differentiation [2,3]. Previous studies have reported that PPAR-γ ligands activate PPAR-γ expressing cells including adipocytes, fibroblasts, myoblasts, and help to induce terminal differentiation. PPAR-γ forms a heterodimeric complex that functions as a central regulator of adipocyte differentiation [7,8]. PPAR-γ is activated by several prostanoids, prostaglandin-like molecules, and arachidonic acid metabolites [3]. Moreover, PPAR-γ ligands induce growth arrest through apoptosis in macrophages and endothelial cells [23]. It has also been reported that PPAR-γ ligands can inhibit growth of several cancer cells *in vitro* and *in vivo* [24–26].

Our Western blot data show that the three prostate cancer cell lines studied here, as well as prostate cancer tissues expressed PPAR-γ. We tested the hypothesis that prostate cancer cells that express PPAR-γ may be inhibited in their proliferation by PPAR-γ ligands. We studied the effects of low and high dose treatments of the PPAR-γ ligands, 15d-PGJ2 and troglitazone on parameters of cell proliferation in three prostate cancer cell lines, LNCaP, PC-3 and DU145. Low concentrations of troglitazone (5 μM) and 15d-PGJ2 (2.5 μM) blocked cell proliferation and suppressed DNA synthesis on all prostate cancer cell lines (Figs. 2 and 3). In addition, we have utilised the selective PPAR-γ antagonist GW9662 to elucidate the involvement of PPAR-γ in the growth inhibitory effects observed. The inhibitory effects

Please cite this article in press as: Nagata D, et al., Peroxisome proliferator-activated receptor-γ and growth inhibition by its ligands in prostate cancer, Cancer Detect Prev (2008), doi:10.1016/j.cdp.2008.05.008

exerted by PPAR-γ ligands were not reversed by the addition of the GW9662 (supplementary data). Our findings demonstrate that the effects induced by 15d-PGJ2 and troglitazone in the prostate cancer cell lines are PPAR-γ independent. The levels of PPAR-γ expression varied significantly amongst the prostate cancer cell lines examined and these differing levels did not associate with the observed growth inhibition. All prostate cancer cell lines showed accumulations of cells in the S-phase after 48 h of treatment with PPAR-γ ligands and no significant increase in the proportion of cells in the G0-G1 phase and the apoptotic phase of cell cycle (Table 2). However, the androgen-dependent cell line, LNCaP, exhibited a lesser effect than the androgen independent cell lines DU145 and PC-3. LNCaP cells grow very slowly in culture and therefore may not have completed an entire cell cycle before the effects of PPAR-γ occur. The completion of cell cycle events in an orderly manner, from the G1 stage to DNA replication in S-phase or from the G2 stage to mitosis, is controlled by many factors, which act as checkpoints to ensure that no mistakes occur [27]. Therefore, in addition to carrying out FACS analysis to study the cell cycle, we also studied changes in the protein expressions of certain cell cycle regulating factors over the time course of 15d-PGJ2 treatment. The cell cycle regulators studied were p53, p21 and p27 all are involved in controlling various checkpoints in the cell cycle. However, no changes were observed in the expression levels of any of these proteins over the time period in which cell cycle arrest occurred (supplementary data).

Additional experiments explored whether PPAR ligands could also inhibit androgen-induced production of PSA. Exposure of LNCaP cells simultaneously to DHT and troglitazone resulted in inhibition of accumulation of PSA protein compared with exposure to DHT alone, as shown by Western blotting (Fig. 5). Reprobing of the Western blot showed that the down-regulation of PSA expression was not mediated through down-regulation of androgen receptor (AR). Because troglitazone is able to inhibit transactivation of a number of secondary signaling pathways, it may be either inhibiting coactivators or stimulating corepressors of the activated AR. A recent report has shown that activated AR requires coactivators for efficient expression of androgen-responsive genes [28,29]. Another less likely hypothesis comes from studies that have shown that induction of immediate early genes such as *c-Jun* and *c-Myc* can be mediated by PPAR-γ ligands and complexes of c-Jun and c-Fos can disrupt transactivation of the ARs [30,31]. Additional studies are clearly required to elucidate the actual mechanism by which PPAR-γ ligands mediate their antiandrogen activities.

The anti-proliferative effects of PPAR-γ ligands cannot totally be explained by inhibition of the androgen-signaling pathway. Prior studies show that PC-3 cells, which have a nonfunctional, mutated AR, are inhibited in their proliferation *in vitro* and *in vivo* by PPAR-γ ligands [32]. In addition, studies by others as well as ourselves have demonstrated that cancer cells from a variety of tissues including colon, breast, fat, and stomach can be inhibited in their proliferation by PPAR-γ ligands; and these cancers are not under androgen control. This would be congruent with the hypothesis that PPAR-γ ligands are affecting key cofactors of activated signaling pathways in these transformed cells.

In this study, we demonstrate that PPAR-γ ligands inhibited proliferation of human prostate cancer cells and transactivation of PSA, suggesting that troglitazone inhibited PSA induction by a mechanism other than down-regulation of the AR. Taken together, these ligands may represent a useful adjuvant therapy for prostate cancer, particularly for patients who have minimal residual disease after surgery or radiotherapy with curative intent.

Acknowledgement

This work was supported by a Grant-in-Aid for Scientific Research (#17591692) from the Ministry of Education, Culture, Sport, Science and Technology of Japan.

Appendix A. Supplementary data

Supplementary data associated with this article can be found, in the online version, at doi:10.1016/j.cdp.2008.05.008.

Conflict of interest

None declared.

References

[1] Jemal A, Murray T, Samuels A, Ghafoor A, Ward E, Thun MJ. Cancer statistics. CA Cancer J Clin 2003; 53:5–26.
[2] Mangelsdorf DJ, Thummel C, Beato M, Herrlich P, Schütz G, Umesono K, et al. The nuclear receptor superfamily: the second decade. Cell 1995; 83:835–9.
[3] Yu K, Bayona W, Kallen CB, Harding HP, Ravera CP, McMahon G, et al. Differential activation of peroxisome proliferator-activated receptors by eicosanoids. J Biol Chem 1995; 270:23975–83.
[4] Qi C, Zhu Y, Reddy JK. Peroxisome proliferator-activated receptors, coactivators, and downstream targets. Cell Biochem Biophys 2000; 32:187–204.
[5] Kliewer SA, Xu HE, Lambert MH, Willson TM. Peroxisome proliferator-activated receptors: from genes to physiology. Recent Prog Horm Res 2001; 56:239–63.
[6] Kim MJ, Deplewski D, Ciletti N, Michel S, Reichert U, Rosenfield RL. Limited cooperation between peroxisome proliferator-activated receptors and retinoid X receptor agonists in sebocyte growth and development. Mol Genet Metab 2001; 74:362–9.
[7] Soret B, Lee HJ, Finley E, Lee SC, Vernon RG. Regulation of differentiation of sheep subcutaneous and abdominal preadipocytes in culture. J Endocrinol 1999; 161:517–24.

Please cite this article in press as: Nagata D, et al., Peroxisome proliferator-activated receptor-γ and growth inhibition by its ligands in prostate cancer, Cancer Detect Prev (2008), doi:10.1016/j.cdp.2008.05.008

[8] Fontaine C, Dubois G, Duguay Y, Helledie T, Vu-Dac N, Gervois P, et al. The orphan nuclear receptor Rev-Erbβ is a peroxisome proliferator-activated receptor (PPAR)-γ target gene and promotes PPAR-γ-induced adipocyte differentiation. J Biol Chem 2003; 278:37672–80.

[9] Mueller E, Sarraf P, Tontonoz P, Evans RM, Martin KJ, Zhang M, et al. Terminal differentiation of human breast cancer through PPAR-γ. Mol Cell 1998; 1:465–70.

[10] Allred CD, Kilogore MW. Selective activation of PPARgamma in breast, colon, and lung cancer cell lines. Mol Cell Endocrinol 2005; 235:21–9.

[11] Nomura S, Nakajima A, Ishimine S, Matsuhashi N, Kadowaki T, Kaminishi M. Differential expression of peroxisome proliferator-activated receptor in histologically different human gastric cancer tissues. J Exp Clin Cancer Res 2006; 25:443–8.

[12] Cesario RM, Stone J, Yen WC, Bissonnette RP, Lamph WW. Differentiation and growth inhibition mediated via the RXR:PPAR-gamma heterodimer in colon cancer. Cancer Lett 2006; 240:225–33.

[13] Kristiansen G, Jacob J, Buckendahl AC, Grutzmann R, Dietel M, Pilarsky C. Peroxisome proliferator-activated receptor gamma is highly expressed in pancreatic cancer and is associated with shorter overall survival times. Clin Cancer Res 2006; 12:6444–51.

[14] Soares AF, Nosjean O, Cozzone D, Lagarde M, Geloen A. Covalent binding of 15-deoxy-delta12,14-prostaglandin J2 to PPAR gamma. Biochem Biophys Res Commun 2005; 337:521–5.

[15] Murphy GJ, Holder JC. PPAR-gamma agonists: therapeutic role in diabetes, inflammation and cancer. Trends Pharmacol Sci 2000; 21:469–74.

[16] Olefsky JM, Saltiel AR. PPAR gamma and the treatment of insulin resistance. Trends Endocrinol Metab 2000; 11:362–8.

[17] Willson TM, Lambert MH, Kliewer SA. Peroxisome proliferator-activated receptor gamma and metabolic disease. Annu Rev Biochem 2001; 70:341–67.

[18] Motomura W, Takahashi N, Nagamine M, Sawamukai M, Tanno S, Kohgo Y, et al. Growth arrest by troglitazone is mediated by p27Kip1 accumulation, which results from dual inhibition of proteasome activity and Skp2 expression in human hepatocellular carcinoma cells. Int J Cancer 2004; 108:41–6.

[19] Han S, Sidell N, Fisher PB, Roman J. Up-regulation of p21 gene expression by peroxisome proliferator-activated receptor gamma in human lung carcinoma cells. Clin Cancer Res 2004; 10:1911–9.

[20] Radhakrishnan SK, Gartel A. The PPAR-gamma agonist pioglitazone post-transcriptionally induces p21 in PC3 prostate cancer but not in other cell lines. Cell Cycle 2005; 4:582–4.

[21] Fujii D, Yoshida K, Tanabe K, Hihara J, Toge T. The ligands of peroxisome proliferator-activated receptor (PPAR) gamma inhibit growth of human esophageal carcinoma cells through induction of apoptosis and cell cycle arrest. Anticancer Res 2004; 24:1409–16.

[22] Nakanishi M, Robetorye RS, Adami GR, Pereira-Smith OM, Smith JR. Identification of the active region of the DNA synthesis inhibitory gene p21 Sdi1/CIP1/WAF1. EMBO J 1995; 14:555–63.

[23] Eligini S, Banfi C, Brambilla M, Camera M, Barbieri SS, Poma F, et al. 15-deoxy-delta12,14-Prostaglandin J2 inhibits tissue factor expression in human macrophages and endothelial cells: evidence for ERK1/2 signaling pathway blockade. Thromb Haemost 2002; 7:524–32.

[24] Kubota T, Koshizuka K, Williamson EA, Asou H, Said JW, Holden S, et al. Ligand for peroxisome proliferator-activated receptor gamma has potent antitumor effects against human prostate cancer both in vitro and in vivo. Cancer Res 1998; 58:3344–52.

[25] Elstner E, Müller C, Koshijuka K, Williamson EA, Park D, Asou H, et al. Ligands for peroxisome proliferator-activated receptor and retinoic acid receptor inhibit growth and induce apoptosis of human breast cancer cells in vitro and in BNX mice. Proc Natl Acad Sci USA 1998; 95:8806–11.

[26] Fulzele SV, Chatterjee A, Shaik MS, Jackson T, Ichite N, Singh M, et al. 15-Deoxy-Delta12,14-prostaglandin J2 enhances docetaxel anti-tumor activity against A549 and H460 non-small-cell lung cancer cell lines and xenograft tumors. Anticancer Drugs 2007; 11:65–78.

[27] Theocharis S, Margeli A, Vielh P, Kouraklis G. Peroxisome proliferator-activated receptor-gamma ligands as cell-cycle modulators. Cancer Treat Rev 2004; 30:545–54.

[28] He B, Gampe RT, Kole AJ, Hnat AT, Stanley TB, An G, et al. Structural basis for androgen receptor interdomain and coactivator interactions suggests a transition in nuclear receptor activation function dominance. Mol Cell 2004; 16:425–38.

[29] Estebanez-Perpina E, Moore JM, Mar E, Webb P, Fletterick RJ, Guy RK. The molecular mechanisms of coactivator utilization in ligand-dependent transactivation by the androgen receptor. J Biol Chem 2005; 280:8060–8.

[30] Edwards J, Krishna NS, Mukherjee R, Bartlett JM. The role of c-Jun and c-Fos expression in androgen-independent prostate cancer. J Pathol 2004; 204:153–8.

[31] Chen SY, Cai C, Fisher CJ, Zheng Z, Omwancha J, Hsieh CL, et al. c-Jun enhancement of androgen receptor transactivation is associated with prostate cancer cell proliferation. Oncogene 2006; 25:7212–23.

[32] Shappell SB, Gupta RA, Manning S, Whitehead R, Boeglin WE, Wheeler TM, et al. 15S-Hydroxyeicosatetraenoic acid activates peroxisome proliferator-activated receptor gamma and inhibits proliferation in PC3 prostate carcinoma cells. Cancer Res 2001; 61:497–503.

Please cite this article in press as: Nagata D, et al., Peroxisome proliferator-activated receptor-γ and growth inhibition by its ligands in prostate cancer, Cancer Detect Prev (2008), doi:10.1016/j.cdp.2008.05.008

Biochemical and Biophysical Research Communications 374 (2008) 79–83

Contents lists available at ScienceDirect

Biochemical and Biophysical Research Communications

journal homepage: www.elsevier.com/locate/ybbrc

Essential role of Chk1 in S phase progression through regulation of RNR2 expression

Hiromichi Naruyama [a,b], Midori Shimada [a], Hiroyuki Niida [a], Doaa H. Zineldeen [a], Yoshihiro Hashimoto [b], Kenjiro Kohri [b], Makoto Nakanishi [a,*]

[a] Department of Cell Biology, Graduate School of Medical Sciences, Nagoya City University, 1 Kawasumi, Mizuho-cho, Mizuho-ku, Nagoya 467-8601, Japan
[b] Department of Urology, Graduate School of Medical Sciences, Nagoya City University, 1 Kawasumi, Mizuho-cho, Mizuho-ku, Nagoya 467-8601, Japan

ARTICLE INFO

Article history:
Received 24 June 2008
Available online 9 July 2008

Keywords:
Cell cycle
Ribonucleotide reductase
Chk1
Transcription
DNA replication

ABSTRACT

Chk1 is an essential kinase for maintaining genome integrity and cell cycle checkpoints through phosphorylating several downstream targets. Recently, we demonstrated that Chk1 is also required for cell proliferation in somatic cells under unperturbed condition through regulating transcription of several genes. Here, we show that Chk1 is required for S phase progression and RNR2 is a critical downstream target of genes transcriptionally regulated by Chk1. Hence, although RNR2 expression reached maximum at S phase in the presence of Chk1, Chk1 depletion arrested the cell cycle at S phase and reduced RNR2 expression at both mRNA and protein levels. Ectopic expression of RNR2 failed to rescue the S phase arrest observed in Chk1 depleted cells, suggesting the presence of an additional Chk1-target(s) for completion of S phase other than RNR2. Therefore, our results suggest that Chk1 is required for DNA replication at least through regulating RNR2 gene transcription.

Progression through the cell cycle is regulated carefully to avoid proliferation or mitosis when adverse conditions exist, such as DNA damage and DNA replication fork stalling [1–3]. Abnormal DNA structures are rapidly sensed and transduced to mediators by either the ATR or ATM PI3-kinase related protein kinases (PIKK) [4,5]. One such mediator is Chk1 kinase that is essential for cell cycle arrest upon DNA damage or DNA replication fork stalling through phosphorylating Cdc25 phosphatases [6,7]. In addition to its role as a checkpoint mediator, Chk1 is a constitutively active enzyme and associates with chromatin under unperturbed condition [8,9]. Chk1 phosphorylates histone H3 at threonine 11 (T11) around the promoter regions of cell cycle regulatory genes including cyclin B1 and Cdk1 [10], which accelerate recruitment of GCN5 histone acetyltransferase and subsequent acetylation at lysine 9 (K9) [11]. Increased acetylation of K9 leads to transcriptional activation.

Ribonucleotide reductase (RNR) is essential for de novo synthesis of deoxyribonucleotides (dNTPs), which are required for DNA replication and repair [12,13]. Most eukaryotic RNRs are composed of two essential and non-identical homodimeric subunits, a large subunit (R1) and a small subunit (R2) [12,14]. The former subunit contains the catalytic site and allosteric regulatory site for both enzyme activity and specificity by binding nucleotide triphosphates [12]. The latter subunit contains a non-heme iron center essential for catalysis. p53-Inducible R2 (53R2) [15], a homologous R2 protein, is also capable of forming an active RNR complex together with the R1 protein [16].

In mammalian cells, the transcription of the R1 and R2 genes is cell cycle dependent, being undetectable in G0/G1 and maximum in S phase [17,18]. The S phase-specific expression of R1 genes is characterized as four different promoter elements, b, a, Inr, and g [19]. Although transcription factor YY1 binds to b and a elements, the cell cycle specific expression is mainly regulated via Inr and g elements. In contrast to R1, the S phase specific expression of R2 is relatively complicated. In mouse cells, S phase-specific transcription of R2 gene requires a repressive E2F-binding site and a promoter-activating region [20]. Interestingly, mutation of the E2F-binding site leads to premature promoter activation in G1 and increase promoter activity. Given that the R1 protein has a long half-life, and its level is apparently constant [21,22] and that the R2 protein is rapidly degraded in mitosis by APC-C [23,24], RNR activity and thus DNA replication are mainly dependent on the level of R2 protein.

In this study, we found that Chk1 depletion results in incomplete S phase, suggesting that Chk1 may be required for transcription of some essential genes for DNA replication. To address this question, we examined changes in the transcription of known genes involved in S phase progression after Chk1 depletion in MEFs. Only

* Corresponding author. Address: Department of Cell Biology, Graduate School of Medical Sciences, Nagoya City University, Kawasumi, Mizuho-cho, Mizuho-ku, Nagoya 467-8601, Japan. Fax: +81 52 842 3955.
E-mail address: mkt-naka@med.nagoya-cu.ac.jp (M. Nakanishi).

0006-291X/$ - see front matter © 2008 Elsevier Inc. All rights reserved.
doi:10.1016/j.bbrc.2008.06.112

RNR2 among genes tested was drastically reduced following loss of Chk1. Therefore, our results suggest an essential function of Chk1 in DNA replication at least through activating RNR2 gene transcription.

Materials and methods

Cells and culture condition. Chk1$^{flox/-}$ MEFs were generated as described previously [10] and were cultured in DMEM supplemented with 10% FBS.

Immunoblotting. Cells were lysed as described previously [10], and extracts were subjected to immunoblotting using anti-Chk1 (sc8408; Santa Cruz), anti-RNR2 (sc10844; Santa Cruz), anti-RNR1 (sc11733; Santa Cruz) antibodies.

Northern blotting. Total RNA was extracted using ISOGEN (Wako) and northern blotting was performed as described previously [25]. ^{32}P-labeled fragment of RNR2 and RNR1 was used as a probe.

Cell cycle analysis. Cells were incubated with 10 μM BrdU for 30 min, harvested, washed once in PBS and fixed with in 70% ethanol. Cells were prepared for FACS analysis as described previously [26].

Real time PCR. Real-time PCR was carried out with single-stranded cDNAs prepared with the SuperScript First-Strand Synthesis System (Invitrogen, Carlsbad, CA, USA). Briefly, total RNA from each sample after transfection was reverse-transcribed with Oligo-dT primer. PCR reactions were performed with Power SYBR Green PCR Master Mix and 7500 Fast Real-Time PCR System (Applied Biosystems, Foster City, CA, USA). Seuence-Specific primers were designed by Primer3 software (http://frodo.wi.mit.edu/cgi-bin/primer3/primer3_www.cgi) as follows; GAPDH, AAC TTTGGCATTGTGGAAGG and GGATGCAGGGATGATGTTCT, Asf1, CAG GCCATTTTACCTTCAGC and GGCTGAGCTTGTTTCTGGAC, MCM4, GACCCTCAGGATGAGGCATA and GGGGCATGATGGTACTATGG, Cdc25C, AAAGACAGGGCTCTGAACCA and TGGTGAAGCATGGGAC AGTA, RNR1, GGTCGTGTCCGAAAAGTTGT and GTTCTGCTGGTTG CTCTTCC RNR2, CGTTGTCTTTCCCATCGAGT and CTCTCATCGGG TTTCAGAGC, Cdc7, GCCCTGCAGAGAAACTCATC and GTTTCCCTC ATCACGCTGTT, Cdc6, TTTCGGAAGTTGATGGGAAC and GGGTCAA AAGCAGCAAAGAG Orc1, ACTGCCATACCCAACCATGT and CAGCA CGTCATTCTGGCTAA, Orc2, TTTGTGCCTTCCTTTTCTGC and CCCA AG CCATAAAGCACAAT, Wee1, GAGAGCTGGAGGACGACTTG and CAGAA AGTAGGCGGTCGAAG, Cdc45, GTTCCTGCCTACGACGACAT and CTC TTCCTGTTTCGCTCCAC. GAPDH primer was used as an internal control. Real-Time PCR was carried out, in duplicate, by 40 cycles of 95 °C for 10 sec and 60 °C for 1 min. Productions of the expected amplification fragments without unanticipated products and primers were confirmed by melting-curve analysis. To determine the relative amounts of the products, we used the comparative Ct (threshold cycle) method according to the instructions supplied by Applied Biosystems. Conventional PCR was performed with the Ex-Taq system (Takara Bio Inc., Shiga, Japan).

Immunohistochemical analysis. Chk1$^{flox/-}$ MEFs were infected with adenoviruses expressing either Cre or LacZ (negative control). Immunohistochemical analyses using anti-RNR1 and anti-RNR2 antibodies were performed as described previously [9].

Results and discussion

Loss of Chk1 resulted in incomplete DNA replication

Recent findings that Chk1 is a histone H3-T11 kinase unravel a mechanism underlying DNA damage-induced transcriptional repression. In this concept, Chk1 is an essential for transcription of some genes under unperturbed condition. Actually, Chk1 depletion in

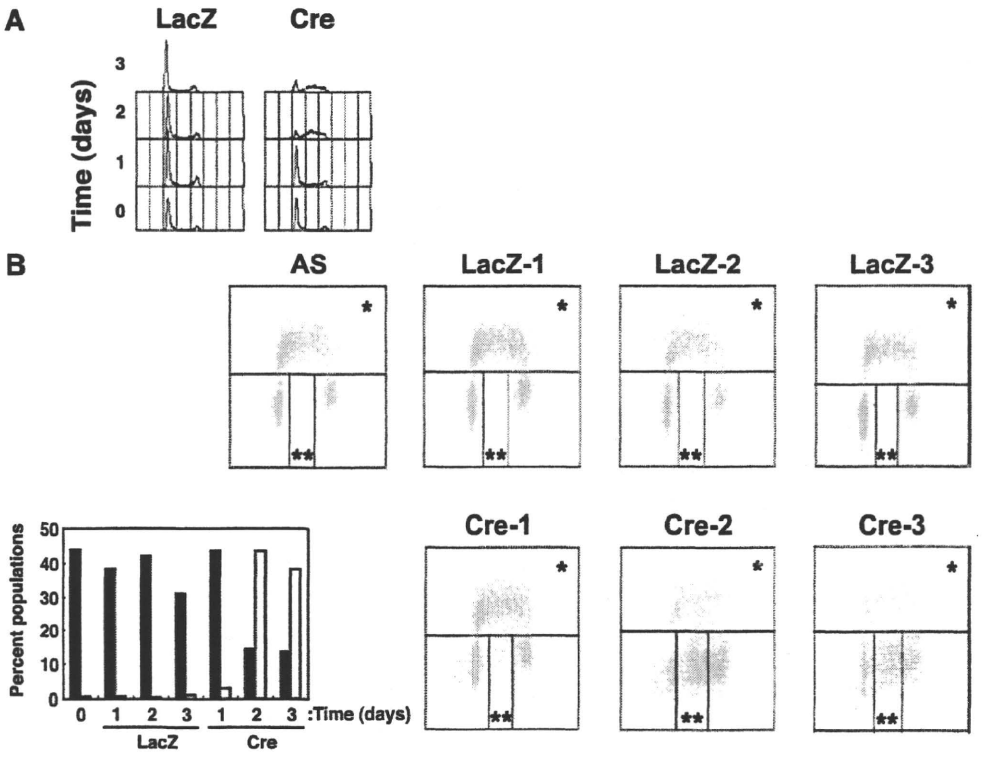

Fig. 1. Chk1 depleted MEFs show S phase arrest. (A) Cell cycle profile of Chk1$^{flox/-}$ and Chk1$^{\Delta/-}$ MEFs at the indicated days after adenoviral infection. (B) Chk1$^{flox/-}$ MEFs were treated with 10 μM BrdU for 30 min before cells were harvested at the time indicated after infection and analysed by FACS. The percentages of BrdU positive (*) and negative (**) cells are shown as a graph (black: BrdU positive; white: BrdU negative).

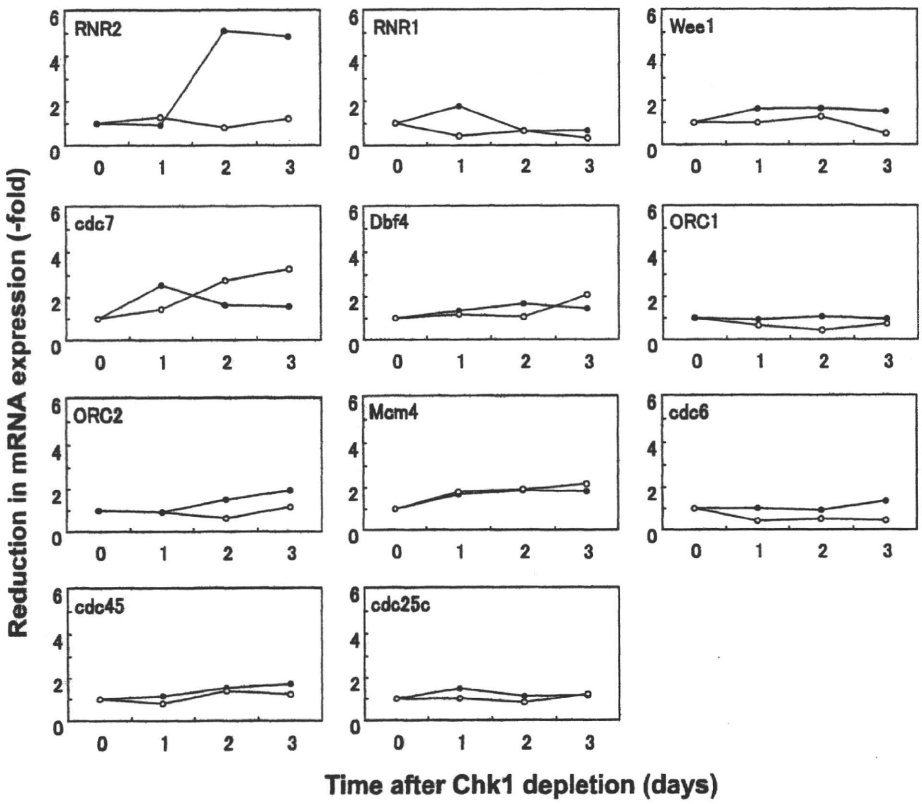

Fig. 2. RNR2 mRNA transcripts were decreased in Chk1 depleted MEFs. Chk1$^{flox/-}$ MEFs were harvested at the indicated times after infection of adenoviruses expressing LacZ (open circles) or Cre (closed circles) and their total RNA was extracted. After treatment with reverse transcriptase using random primers, real time PCR was performed using their specific primers to measure the transcripts involved in DNA replication or cell cycle control. The results are presented as a fold-reduction of controls (before infection of adenoviruses).

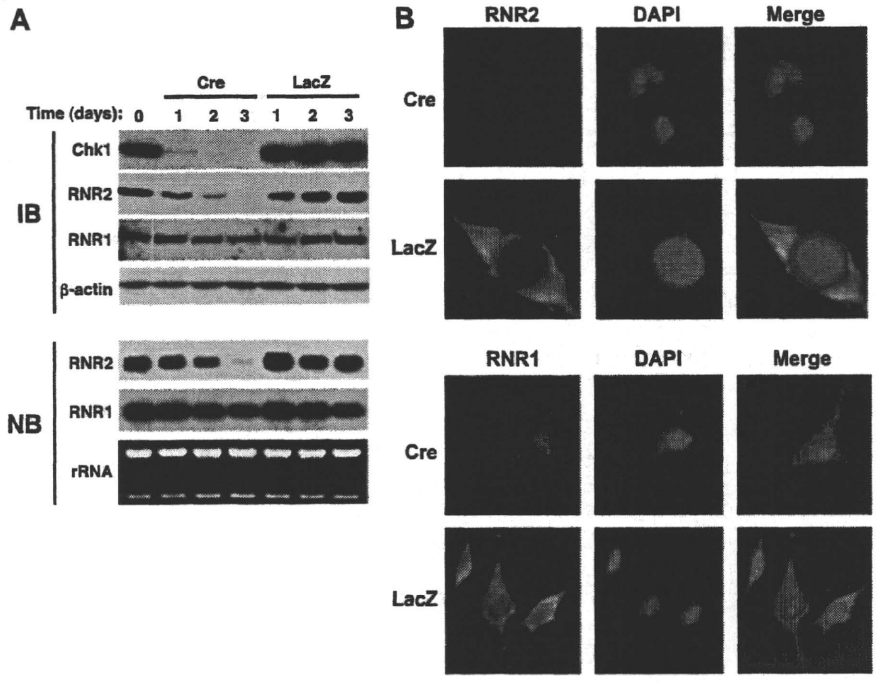

Fig. 3. Specific reduction in RNR2 protein in Chk1 depleted MEFs. Chk1$^{flox/-}$ MEFs were harvested at the indicated times after infection of adenoviruses expressing LacZ or Cre. The resultant whole cell extracts and total RNA were prepared and subjected to immunoblotting (IB) using the indicated antibodies or northern blotting (NB) analysis using RNR2 or RNR1 probes. (B) Immunohistochemical analysis of RNR2 and RNR1 in Chk1 depleted cells. Chk1$^{flox/-}$ MEFs were infected with adenoviruses expressing either LacZ or Cre. Three days after infection the resultant cells were fixed and stained with anti-RNR2 or anti-RNR1 antibodies. Cells were also counterstained with DAPI.